Angular momentum conservation and phonon spin in magnetic insulators

Andreas Rückriegel,[1] Simon Streib,[2] Gerrit E. W. Bauer,[2,3] and Rembert A. Duine[1,4,5]

[1]*Institute for Theoretical Physics and Center for Extreme Matter and Emergent Phenomena, Utrecht University, Leuvenlaan 4, 3584 CE Utrecht, The Netherlands*

[2]*Kavli Institute of NanoScience, Delft University of Technology, Lorentzweg 1, 2628 CJ Delft, The Netherlands*

[3]*Institute for Materials Research & WPI-AIMR & CSRN, Tohoku University, Sendai 980-8577, Japan*

[4]*Center for Quantum Spintronics, Department of Physics, Norwegian University of Science and Technology, NO-7491 Trondheim, Norway*

[5]*Department of Applied Physics, Eindhoven University of Technology, P.O. Box 513, 5600 MB Eindhoven, The Netherlands*

(Received 23 December 2019; accepted 17 February 2020; published 2 March 2020)

We develop a microscopic theory of spin-lattice interactions in magnetic insulators, separating rigid-body rotations and the internal angular momentum, or spin, of the phonons, while conserving the total angular momentum. In the low-energy limit, the microscopic couplings are mapped onto experimentally accessible magnetoelastic constants. We show that the transient phonon spin contribution of the excited system can dominate over the magnon spin, leading to nontrivial Einstein-de Haas physics.

DOI: 10.1103/PhysRevB.101.104402

I. INTRODUCTION

The discovery of the spin Seebeck effect led to renewed interest in spin-lattice interactions in magnetic insulators [1,2], i.e., the spin current generation by a temperature gradient, which is strongly affected by lattice vibrations [3–7]. The spin-lattice interaction is also responsible for the dynamics of the angular momentum transfer between the magnetic order and the underlying crystal lattice that supports both rigid-body dynamics and lattice vibrations, i.e., phonons. In the Einstein-de Haas [8] and Barnett effects [9], a change of magnetization induces a global rotation and vice versa. While both effects have been discovered more than a century ago, their dynamics and the underlying microscopic mechanisms are still under debate [10–13].

In 1962 Vonsovskii and Svirskii [14,15] suggested that circularly polarized transverse phonons can carry angular momentum, analogous to the spin of circularly polarized photons. This prediction was confirmed recently by Holanda *et al.* [16] by Brillouin light scattering on magnetic films in magnetic field gradients that exposed spin-coherent magnon-phonon conversion. Ultrafast demagnetization experiments can be explained only by the transfer of spin from the magnetic system to the lattice on subpicosecond time scales in the form of transverse phonons [12]. Theories address the phonon spin induced by Raman spin-phonon interactions [17], by the relaxation of magnetic impurities [11,18], by temperature gradients in magnets with broken inversion symmetry [19], and phonon spin pumping into nonmagnetic contacts by ferromagnetic resonance dynamics [20]. The phonon Zeeman effect has also been considered [21]. The quantum dynamics of magnetic rigid rotors has been investigated recently in the context of levitated nanoparticles [22–25]. Very recently ferromagnetic resonance experiments have shown coherent magnon-phonon coupling over millimeter distances [26].

Most theories of spin-lattice interactions do not conserve angular momentum [11,27,28], thereby assuming the existence of a sink for angular momentum. The magnetocrystalline anisotropy breaks the spin rotational invariance by imposing a preferred magnetization direction relative to the crystal lattice, while the lattice dynamics itself is described in terms of spinless phonons. The resulting loss of angular momentum conservation is justified when the spin-phonon Hamiltonian does not possess rotational invariance in the first place [11], e.g., by excluding rigid-body dynamics of the lattice and/or by boundary conditions that break rotational invariance. In the absence of such boundary conditions, the angular momentum must be conserved in all spin-lattice interactions. Phenomenological theories that address this issue [10,11,18,29–33] incorporate infinitesimal lattice rotations due to phonons but do not allow for global rigid-body dynamics and therefore cannot describe the physics of the Einstein-de Haas and Barnett effects. Conversely, theories addressing specifically Einstein-de Haas and Barnett effects usually disregard effects of phonons beyond magnetization damping [34–37].

Here we develop a theory of the coupled spin-lattice dynamics for sufficiently large but finite particles of a magnetic insulator allowing for global rotations. We proceed from a microscopic Hamiltonian that conserves the total angular momentum. We carefully separate rigid-body dynamics and phonons, which allows us to define a phonon spin and to obtain the mechanical torques exerted by the magnetic order on the rigid-body and the phonon degrees of freedom (and vice versa). The theory of magnetoelasticity is recovered as the low-energy limit of our microscopic model in the body-fixed frame and thereby reconciled with angular momentum conservation. We compute the nonequilibrium spin dynamics of a bulk ferromagnet subject to heating and spin pumping in linear response and find that in nonequilibrium the phonons carry finite spin, viz. a momentum imbalance between the two circularly polarized transverse phonon modes. We also show that the phonon spin can have nontrivial effects on the rigid-body rotation; in particular, it can lead to an experimentally

observable, transient change in the sense of rotation during equilibration.

The rest of the paper is organized as follows: The spin-lattice Hamiltonian and the decoupling of rigid-body dynamics and phonons is presented in Sec. II. The spin transfer in a bulk ferromagnet is studied in Sec. III within linear response theory. Section IV contains a discussion of our results and concluding remarks. Expressions for the total angular momentum operator in terms of the Euler angles of the rigid-body rotation are presented in Appendix A, while Appendix B details the phonon commutation relations in finite systems. Finally, Appendix C addresses the relaxation rates computed by linear response.

II. MICROSCOPIC SPIN-LATTICE HAMILTONIAN

We address here a finite magnetic insulator of N atoms (or clusters of atoms) with masses m_i and spin operators $\boldsymbol{S}_i$ governed by the Hamiltonian

$$H = \sum_{i=1}^{N} \frac{\boldsymbol{p}_i^2}{2m_i} + V(\{\boldsymbol{r}_i\}) + V_{\text{ext}}(\{\boldsymbol{r}_i\}) + H_S, \tag{1}$$

where $\boldsymbol{r}_i$ and $\boldsymbol{p}_i$ are the canonical position and momentum operators of the ith atom, and the potential $V(\{\boldsymbol{r}_i\})$ is assumed to be (Euclidean) invariant to translations and rotations of the whole body. $V_{\text{ext}}(\{\boldsymbol{r}_i\})$ accounts for external mechanical forces acting on the body. Because of translational and rotational invariance, the spin Hamiltonian H_S depends only on $\boldsymbol{r}_{ij} = \boldsymbol{r}_i - \boldsymbol{r}_j$ and must be a scalar under simultaneous rotations of lattice and spin degrees of freedom. Since $\boldsymbol{S}_i$ are pseudovectors and $\boldsymbol{r}_{ij}$ are vectors, the spin-lattice interaction depends only on $r_{ij} = \sqrt{\boldsymbol{r}_{ij}^2}$, $\boldsymbol{S}_i \cdot \boldsymbol{S}_j$ and even powers of $\boldsymbol{S}_i \cdot \boldsymbol{r}_{ij}$.[1] Considering only pair interactions between two spins, we arrive at $H_S = H_{\text{Ex}} + H_{\text{A}} + H_{\text{Z}}$, with exchange (Ex), anisotropy (A), and Zeeman (Z) contributions

$$H_{\text{Ex}} = -\frac{1}{2} \sum_{\substack{i,\, j\, =\, 1 \\ i \neq j}}^{N} J(r_{ij}) \boldsymbol{S}_i \cdot \boldsymbol{S}_j, \tag{2a}$$

$$H_{\text{A}} = -\frac{1}{2} \sum_{i,j=1}^{N} K(r_{ij}) (\boldsymbol{S}_i \cdot \boldsymbol{r}_{ij})(\boldsymbol{S}_j \cdot \boldsymbol{r}_{ij}), \tag{2b}$$

$$H_{\text{Z}} = -\gamma \boldsymbol{B} \cdot \sum_{i=1}^{N} \boldsymbol{S}_i. \tag{2c}$$

Here $J(r_{ij})$ is an isotropic and $K(r_{ij})$ an anisotropic exchange interaction, $\boldsymbol{B}$ is the external magnetic field, and $\gamma = g\mu_B/\hbar$ is the (modulus of the) gyromagnetic ratio, defined in terms of the g factor and Bohr magneton μ_B, and Planck's constant $\hbar$. H_{A} encodes the interaction of the spins with the crystal lattice or crystalline anisotropy, which in the long-wavelength limit reduces to the conventional crystal field Hamiltonian in terms of anisotropy and magnetoelastic constants [27,28] (see Sec. II B). The interactions $J(r_{ij})$ and $K(r_{ij})$ in principle include dipolar interactions. A Hamiltonian of the form of Eq. (2) has been used recently to compute the relaxation of a classical spin system [38].

Ultimately, the origin of the Hamiltonian (2) lies in the spin-orbit coupling of the electrons: The anisotropic contribution (2b) arises from the dynamical crystal field that affects the electronic orbitals and thereby the spin states, whereas the position dependence of the exchange contribution (2a) is due to the dependence of the electronic hopping integrals on the interatomic distances. For ultrafast processes that occur on the timescales of the orbital motion, a description of these intermediate, electronic stages of the spin-lattice coupling might be necessary; however, this is beyond the scope of this work.

A. Rigid-body rotations and phonon spin

The Hamiltonian (1) commutes with and thereby conserves the total angular momentum, i.e., the sum of intrinsic electron spin and mechanical angular momentum. In a solid, the mechanical angular momentum arises from the rotation of the rigid lattice and the internal phonon dynamics. We may decouple the 6 rigid-body and the $3N - 6$ phonon degrees of freedom by the following transformation:

$$\boldsymbol{r}_i = \boldsymbol{R}_{\text{CM}} + \mathcal{R}(\phi, \theta, \chi) \left[\boldsymbol{R}_i + \sum_{n=1}^{3N-6} \frac{\boldsymbol{f}_n(\boldsymbol{R}_i)}{\sqrt{m_i}} q_n \right], \tag{3}$$

where $\boldsymbol{R}_{\text{CM}}$ is the center-of-mass position, $\mathcal{R}(\phi, \theta, \chi) = \mathcal{R}_z(\phi)\mathcal{R}_y(\theta)\mathcal{R}_x(\chi)$ is a three-dimensional rotation parametrized by the Euler angles ϕ, θ, and χ ($\mathcal{R}_\mu(\alpha)$ denoting a rotation by an angle α around an axis $\hat{\boldsymbol{e}}_\mu$), $\boldsymbol{R}_i$ is the body-fixed equilibrium position of the ith particle, and the q_n are the normal coordinates of the lattice, i.e., the phonons, with eigenfunctions $\boldsymbol{f}_n(\boldsymbol{R}_i)$ that diagonalize the energy to second order in q_n:

$$V(\{\boldsymbol{r}_i\}) = V(\{\boldsymbol{R}_i\}) + \frac{1}{2} \sum_{n=1}^{3N-6} \omega_n^2 q_n^2 + \mathcal{O}(q^3). \tag{4}$$

In molecular physics this decoupling of rotations and vibrations is referred to as Eckart convention [39–41]. Neglecting surface effects of the external forces on the phonons, we also have $V_{\text{ext}}(\{\boldsymbol{r}_i\}) \approx V_{\text{ext}}(\boldsymbol{R}_{\text{CM}}, \phi, \theta, \phi)$.

Since we describe the phonons within a rotating reference frame, it is advantageous to also rotate the spin operators globally by the unitary transformation:

$$U(\phi, \theta, \chi) = e^{-\frac{i}{\hbar}\phi \sum_{j=1}^{N} S_j^z} e^{-\frac{i}{\hbar}\theta \sum_{j=1}^{N} S_j^y} e^{-\frac{i}{\hbar}\chi \sum_{j=1}^{N} S_j^x}, \tag{5}$$

so that $U^\dagger(\phi, \theta, \chi)\boldsymbol{S}_i U(\phi, \theta, \chi) = \mathcal{R}(\phi, \theta, \chi)\boldsymbol{S}_i$. As a result, (3) and (5) transform $\boldsymbol{r}_i$ into $\boldsymbol{R}_i + \sum_{n=1}^{3N-6} \frac{\boldsymbol{f}_n(\boldsymbol{R}_i)}{\sqrt{m_i}} q_n$ and $\boldsymbol{B}$ into $\mathcal{R}^T(\phi, \theta, \chi)\boldsymbol{B}$ in the spin Hamiltonian (2) and change the lattice kinetic energy to [40–42]

$$\sum_{i=1}^{N} \frac{\boldsymbol{p}_i^2}{2m_i} \to \frac{\boldsymbol{P}_{\text{CM}}^2}{2M} + \frac{1}{2} \boldsymbol{\Omega} \cdot \mathbf{I} \cdot \boldsymbol{\Omega} + \frac{1}{2} \sum_{n=1}^{3N-6} p_n^2 + \mathcal{O}(I^{-2}). \tag{6}$$

Here, $\boldsymbol{P}_{\text{CM}} = -i\hbar\partial/\partial \boldsymbol{R}_{\text{CM}}$ and $p_n = -i\hbar\partial/\partial q_n$ are the momentum operators of center-of-mass translation and

[1] Broken inversion symmetry would allow Dzyaloshinskii-Moriya interactions of the form $(\boldsymbol{r}_{il} \times \boldsymbol{r}_{jl}) \cdot (\boldsymbol{S}_i \times \boldsymbol{S}_j)$.

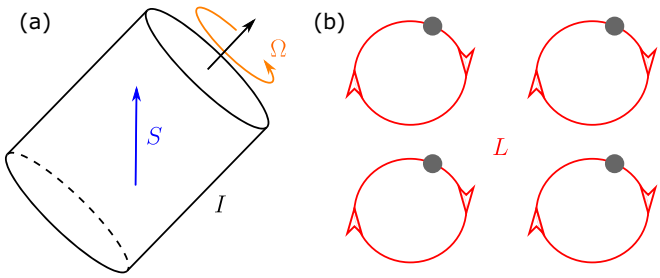

FIG. 1. Illustration of the different kinds of angular momenta that are relevant for the angular momentum balance (7) of a magnetic insulator: (a) Rigid rotation with angular velocity $\boldsymbol{\Omega}$ of a cylinder around its axis with moment of inertia I and total spin $\boldsymbol{S}$, (b) sketch of a phonon mode with angular momentum $\boldsymbol{L}$, showing the motion of four different volume elements without a global rotation as in (a). The total angular momentum is $\boldsymbol{J} = \mathbf{I}\cdot\boldsymbol{\Omega} + \boldsymbol{L} + \boldsymbol{S}$.

phonons, respectively, $M = \sum_{i=1}^{N} m_i$ is the total mass, and $\mathbf{I}$ is the equilibrium moment of inertia tensor $I^{\alpha\beta} = \sum_{i=1}^{N} m_i(\delta^{\alpha\beta}\boldsymbol{R}_i^2 - R_i^{\alpha}R_i^{\beta})$. The latter is defined in the frame attached to and rotating with the body, referred to as "rotating," "molecular," or "body-fixed" frame. $\mathcal{O}(I^{-2})$ denotes correction terms originating from instantaneous phonon corrections to the moment of inertia and quantum-mechanical commutators generated by the nonlinear coordinate transformation (3) [40–42]. Finally,

$$\boldsymbol{\Omega} = \mathbf{I}^{-1}\cdot(\boldsymbol{J} - \boldsymbol{L} - \boldsymbol{S}) \tag{7}$$

is the vector of the angular velocity of the rigid rotation in the body-fixed reference frame. Here the total and phonon angular momentum operators $\boldsymbol{J}$ and $\boldsymbol{L}$, and the total spin operator $\boldsymbol{S} = \sum_{i=1}^{N} \boldsymbol{S}_i$ are also in the body-fixed coordinate system. The three angular momenta in a magnetic insulator are sketched in Fig. 1. The total angular momentum in the laboratory frame $\boldsymbol{J}_{\text{lab}} = \mathcal{R}(\phi,\theta,\chi)\boldsymbol{J}$ obeys the standard angular momentum algebra $[J^x_{\text{lab}}, J^y_{\text{lab}}] = i\hbar J^z_{\text{lab}}$ and is conserved in the absence of external torques, i.e., for $\boldsymbol{B} = 0$ and $[\boldsymbol{J}, V_{\text{ext}}] = 0$. The total angular momentum in the body-fixed frame depends only on the Euler angles, i.e., it is carried solely by the rigid-body rotation [40] and the angular momentum commutation relations are anomalous (with negative sign) $[J^x, J^y] = -i\hbar J^z$ [40–43]. Explicit expressions for the total angular momentum operators in the body-fixed and laboratory frame are relegated to Appendix A. The "phonon spin" is the phonon angular momentum in the body-fixed frame:

$$\boldsymbol{L} = \sum_{i=1}^{N} \boldsymbol{l}_i = \sum_{i=1}^{N} \boldsymbol{u}_i \times \boldsymbol{\pi}_i, \tag{8}$$

where $\boldsymbol{u}_i$ and $\boldsymbol{\pi}_i$ are, respectively, the displacement and linear momentum operators:

$$\boldsymbol{u}_i = \frac{1}{\sqrt{m_i}} \sum_{n=1}^{3N-6} \boldsymbol{f}_n(\boldsymbol{R}_i) q_n, \tag{9a}$$

$$\boldsymbol{\pi}_i = \sqrt{m_i} \sum_{n=1}^{3N-6} \boldsymbol{f}_n(\boldsymbol{R}_i) p_n. \tag{9b}$$

Care has to be exercised when interpreting the phonon operators (9) and (8) in a finite system. The exclusion of the 6 degrees of freedom of the rigid-body dynamics breaks the canonical commutation relations of the phonon position, momentum, and angular momentum operators. Corrections of $\mathcal{O}(I^{-1})$ [42] are important for nanoscale systems. For details of the derivation of the kinetic energy (6) and the finite size corrections, we refer to Refs. [40–42]. In the following, we focus on systems large enough, i.e., $N \gg 1$ as shown in Appendix B, to disregard finite size corrections to $\boldsymbol{L}$'s thermal or quantum fluctuations and treat the phonon operators (9) and (8) canonically.

The equations of motion of the relevant angular momentum operators are now

$$\partial_t \boldsymbol{S} + \frac{1}{2}(\boldsymbol{\Omega}\times\boldsymbol{S} - \boldsymbol{S}\times\boldsymbol{\Omega}) = \boldsymbol{S}\times\mathcal{R}^T(\phi,\theta,\chi)\gamma\boldsymbol{B} + \sum_{i=1}^{N}(\boldsymbol{R}_i + \boldsymbol{u}_i)\times\frac{\partial H_S}{\partial \boldsymbol{u}_i}, \tag{10a}$$

$$\partial_t \boldsymbol{L} + \frac{1}{2}(\boldsymbol{\Omega}\times\boldsymbol{L} - \boldsymbol{L}\times\boldsymbol{\Omega}) = -\sum_{i=1}^{N}\boldsymbol{u}_i\times\left(\frac{\partial V}{\partial \boldsymbol{u}_i} + \frac{\partial H_S}{\partial \boldsymbol{u}_i}\right), \tag{10b}$$

$$\partial_t \boldsymbol{J} + \frac{1}{2}(\boldsymbol{\Omega}\times\boldsymbol{J} - \boldsymbol{J}\times\boldsymbol{\Omega}) = \boldsymbol{S}\times\mathcal{R}^T(\phi,\theta,\chi)\gamma\boldsymbol{B} + \boldsymbol{\mathcal{T}}_{\text{ext}}, \tag{10c}$$

where $\boldsymbol{\mathcal{T}}_{\text{ext}} = -i[\boldsymbol{J}, V_{\text{ext}}]/\hbar$ is the external mechanical torque that acts on the magnet in the body-fixed frame. Thus, the angular momentum $\mathbf{I}\cdot\boldsymbol{\Omega}$ of the rigid rotation satisfies

$$\partial_t(\mathbf{I}\cdot\boldsymbol{\Omega}) + \frac{1}{2}[\boldsymbol{\Omega}\times(\mathbf{I}\cdot\boldsymbol{\Omega}) - (\mathbf{I}\cdot\boldsymbol{\Omega})\times\boldsymbol{\Omega}] = \boldsymbol{\mathcal{T}}_{\text{ext}} - \sum_{i=1}^{N}\left(\boldsymbol{R}_i\times\frac{\partial H_S}{\partial \boldsymbol{u}_i} - \boldsymbol{u}_i\times\frac{\partial V}{\partial \boldsymbol{u}_i}\right). \tag{11}$$

Equations (10) and (11) constitute the microscopic equations for the Einstein-de Haas [8] and Barnett [9] effects in magnetic insulators. The left-hand sides are covariant derivatives that account for the change in angular momentum in the body-fixed frame [41], whereas the right-hand sides are the internal mechanical (V), spin-lattice (H_S), and external magnetic ($\boldsymbol{B}$) and mechanical ($\boldsymbol{\mathcal{T}}_{\text{ext}}$) torques. The spins exert a torque on the lattice by driving the rigid-body rotation and exciting phonons. The torques on the right-hand sides depend on the microscopic phonon and spin degrees of freedom that act as thermal baths and thereby break time-reversal symmetry. We disregard radiative damping, so energy is conserved and entropy cannot decrease, in contrast to conventional approaches to the Einstein-de Haas effect that demand angular momentum conservation only and do not include thermal baths. Hence, energy is not conserved in these approaches and entropy can decrease.

B. Derivation of the phenomenological theory of magnetoelasticity

Our general model for spin-lattice interactions can be parametrized by a small number of magnetic and

magnetoelastic constants at low energies. In the long wavelength continuum limit $\boldsymbol{S}_i \to \boldsymbol{S}(\boldsymbol{r})/n$ and $\boldsymbol{u}_i \to \boldsymbol{u}(\boldsymbol{r})$, where n is the number density of magnetic moments. To lowest order in the gradients of spin and phonon operators

$$H_{\mathrm{Ex}} \approx \frac{n}{\hbar^2 s^2}\int \mathrm{d}^3 r \sum_{\mu\nu}\left[\frac{J_{\mu\nu}}{2} + \sum_{\alpha\beta} A_{\mu\nu\alpha\beta}\epsilon^{\alpha\beta}(\boldsymbol{r}) + \ldots\right] \times \frac{\partial \boldsymbol{S}(\boldsymbol{r})}{\partial r^{\mu}} \cdot \frac{\partial \boldsymbol{S}(\boldsymbol{r})}{\partial r^{\nu}}, \tag{12a}$$

$$H_{\mathrm{A}} \approx \frac{n}{\hbar^2 s^2}\int \mathrm{d}^3 r \sum_{\mu\nu}\left[-\frac{K_{\mu\nu}}{2} + \sum_{\alpha\beta} B_{\mu\nu\alpha\beta}\epsilon^{\alpha\beta}(\boldsymbol{r}) + \ldots\right] \times \tilde{S}^{\mu}(\boldsymbol{r})\tilde{S}^{\nu}(\boldsymbol{r}), \tag{12b}$$

where $s = Sn$ is the saturation spin density in units of $\hbar$,

$$\epsilon^{\alpha\beta}(\boldsymbol{r}) = \frac{1}{2}\left[\frac{\partial u^{\beta}(\boldsymbol{r})}{\partial r^{\alpha}} + \frac{\partial u^{\alpha}(\boldsymbol{r})}{\partial r^{\beta}} + \frac{\partial \boldsymbol{u}(\boldsymbol{r})}{\partial r^{\alpha}} \cdot \frac{\partial \boldsymbol{u}(\boldsymbol{r})}{\partial r^{\beta}}\right] \tag{13}$$

is the elastic strain tensor,

$$\tilde{S}^{\mu}(\boldsymbol{r}) = \left[S^{\mu}(\boldsymbol{r}) + \boldsymbol{S}(\boldsymbol{r}) \cdot \frac{\partial \boldsymbol{u}(\boldsymbol{r})}{\partial r^{\mu}}\right] \tag{14}$$

are the projections of the spin density on the elastically deformed anisotropy axes, and the ellipses stand for higher powers of the strain tensor. Exchange, anisotropy, and magnetoelastic constants can be expressed as moments of the isotropic (J) and anisotropic (K) exchange interactions and their spatial derivatives $J'(R) = \partial J(R)/\partial R$ and $K'(R) = \partial K(R)/\partial R$:

$$J_{\mu\nu} = \frac{\hbar^2 s^2}{2n^2}\sum_i J(R_i) R_i^{\mu} R_i^{\nu}, \tag{15a}$$

$$K_{\mu\nu} = \frac{\hbar^2 s^2}{n^2}\sum_i K(R_i) R_i^{\mu} R_i^{\nu}, \tag{15b}$$

$$A_{\mu\nu\alpha\beta} = \frac{\hbar^2 s^2}{4n^2}\sum_i \frac{J'(R_i)}{R_i} R_i^{\mu} R_i^{\nu} R_i^{\alpha} R_i^{\beta} \tag{15c}$$

$$B_{\mu\nu\alpha\beta} = -\frac{\hbar^2 s^2}{2n^2}\sum_i \frac{K'(R_i)}{R_i} R_i^{\mu} R_i^{\nu} R_i^{\alpha} R_i. \tag{15d}$$

The continuum limit (12) agrees with the standard, phenomenological theory of magnetoelasticity [27]. Equation (12b) includes the spin-lattice coupling by rotational strains [11] via the spin density projections $\tilde{S}^{\mu}(\boldsymbol{r})$.

The exchange, anisotropy, and magnetoelastic constants (15) reflect the microscopic crystal symmetries. For a simple cubic lattice with lattice constant $a = n^{-1/3}$, and nearest-neighbor isotropic as well as next-nearest-neighbor anisotropic exchange we find $J_{\mu\nu} = SJ_s\delta_{\mu\nu}$ and $K_{\mu\nu} = K\delta_{\mu\nu}$, with spin stiffness $J_s = \hbar^2 SJ(a)a^2$ and anisotropy constant $K = 2\hbar^2 S^2[K(a) + 4K(\sqrt{2}a)]a^2$. The latter may be disregarded because it only adds a constant to the Hamiltonian. The magnetoelastic coupling constants become $A_{\mu\nu\alpha\beta} = A_{\parallel}\delta_{\mu\nu}\delta_{\nu\alpha}\delta_{\alpha\beta}$, and $B_{\mu\nu\alpha\beta} = (B_{\parallel} - \frac{3}{2}B_{\perp})\delta_{\mu\nu}\delta_{\nu\alpha}\delta_{\alpha\beta} + \frac{1}{2}B_{\perp}(\delta_{\mu\nu}\delta_{\alpha\beta} + \delta_{\mu\alpha}\delta_{\nu\beta} + \delta_{\mu\beta}\delta_{\nu\alpha})$, with $A_{\parallel} = \frac{\hbar^2 S^2}{2}J'(a)$, $B_{\parallel} = -\hbar^2 S^2[K'(a) + \sqrt{2}K'(\sqrt{2}a)]a^3$, and $B_{\perp} = -2\sqrt{2}\hbar^2 S^2 K'(\sqrt{2}a)a^3$. The anisotropy parameters $B_{\parallel}$ and $B_{\perp}$ are known for many magnets [27]. The exchange-induced magnetoelastic constant can be estimated as $A_{\parallel} \approx \frac{3}{2}\Gamma_m SJ_s$ [7], where $\Gamma_m = \partial \ln T_C/\partial \ln V$ is the magnetic Grüneisen parameter that quantifies the change of Curie temperature T_C with the volume V.

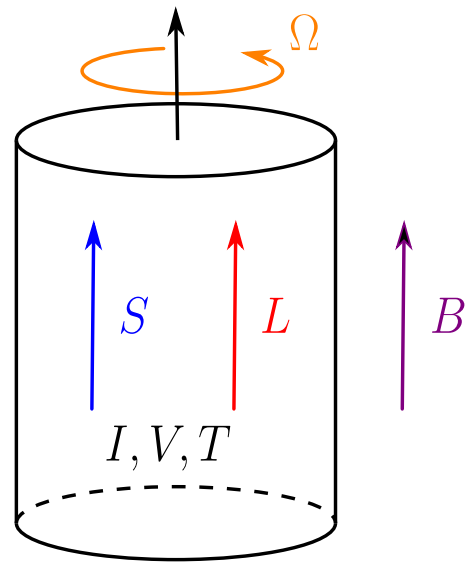

FIG. 2. The system under consideration in Sec. III: A macroscopic ferromagnet with moment of inertia I and volume V at temperature T. The total spin $\boldsymbol{S}$ of the ferromagnet is aligned parallel to an external magnetic field $\boldsymbol{B}$. In addition, the ferromagnet may rotate with angular velocity $\boldsymbol{\Omega}$ and supports a phonon spin $\boldsymbol{L}$. The system is assumed to be at rest with $\boldsymbol{\Omega} = 0$ initially. Finite $\boldsymbol{\Omega}$ and $\boldsymbol{L}$ are induced by exciting the system into a nonequilibrium state at time $t = 0$, e.g., by heating the phonons or by pumping the magnons with an rf field. In this case both $\boldsymbol{\Omega}$ and $\boldsymbol{L}$ are parallel to the total spin $\boldsymbol{S}$ because of the conservation of total angular momentum.

III. THERMAL SPIN TRANSFER

In the remainder of this paper, we focus on a particular application of the general theory, viz. the angular momentum transfer by thermal fluctuations in the bulk of a macroscopic, externally excited, levitated ferromagnetic particle that does not rotate ($\langle\boldsymbol{\Omega}\rangle = 0$) initially. We assume a simple cubic lattice at low temperatures. The average magnetic order parameter, i.e., the total spin $\boldsymbol{S}$, is aligned to an external magnetic field $\boldsymbol{B} = B\hat{\boldsymbol{e}}_z$. For convenience we chose an axially symmetric setup as sketched in Fig. 2. Local spin fluctuations are described via the leading order Holstein-Primakoff transformation [44]

$$S_i^{+} = (S_i^{-})^{\dagger} = \hbar\sqrt{2S}[b_i + \mathcal{O}(1/S)], \tag{16a}$$

$$S_i^{z} = \hbar(S - b_i^{\dagger}b_i), \tag{16b}$$

where $b_i^{\dagger}(b_i)$ is the magnon creation (annihilation) operator on site i, which satisfies the Boson commutation relations $[b_i, b_j^{\dagger}] = \delta_{ij}$.

In a macroscopic magnet the time scales between the rigid-body rotation and the internal magnon and phonon dynamics are decoupled: For a system with volume V, the moment of inertia $I \sim V^{5/3}$, whereas the angular momentum

operators $\boldsymbol{J}$, $\boldsymbol{L}$, and $\boldsymbol{S}$ are extensive quantities, proportional to V. According to Eq. (7) the angular velocity $\boldsymbol{\Omega}$ scales as $V^{-2/3}$. On the other hand, the lowest phonon frequency $\omega_{\min} \sim V^{-1/3}$, while the magnon gap is controlled by external magnetic and internal anisotropy fields and is typically of the order of 10 GHz independent of V. For sufficiently large systems and weak driving, inertial forces of the rigid-body rotation therefore affect the dynamics of both magnons and phonons only negligibly and can be disregarded. By the same argument, the energy $\frac{1}{2}\boldsymbol{\Omega}\cdot\mathbf{I}\cdot\boldsymbol{\Omega} \sim V^{1/3}$ of the rigid-body rotation is small compared to the total magnon and phonon energies $\sim V$. Energy is then (almost) exclusively equilibrated by spin-phonon interactions, under the constraint of angular momentum conservation that includes the rigid-body rotation. For example, consider the change in energy of the magnet at rest when a single magnon with frequency ϵ is removed from the system, which increases the spin by $\Delta S = \hbar$. If this angular momentum is fully transferred to the rigid rotation of a sphere with scalar moment of inertia I, $\Delta L_R = -\hbar = I\Omega^z$. For a macroscopic magnet the change of rotational energy $\Delta E_R = \hbar^2/2I$ is negligible compared to the magnetic energy change $\Delta E_m = -\hbar\epsilon$, since the typical magnon frequencies are in the GHz-THz range, whereas both Ω^z and I^{-1} are small by some power of the inverse volume. Consequently, the energy of the magnon cannot be transferred completely to the rigid rotation, since both energy and angular momentum cannot be conserved simultaneously. The Einstein-de Haas effect can therefore not exist without an intermediate bath, which in magnetic insulators can only be the lattice vibrations.

At temperatures sufficiently below the Curie and Debye temperatures and weak external excitation, only the long-wavelength modes are occupied and Eq. (12) is appropriate. At not too low temperatures we may also disregard magnetodipolar interactions [7]. We assume again that the magnet is sufficiently large that surface effects are small and the eigenmodes of the system may be approximated by plane waves. Then the Fourier transform $b_i = N^{-1/2}\sum_{\boldsymbol{k}} e^{-i\boldsymbol{k}\cdot\boldsymbol{R}_i} b_{\boldsymbol{k}}$ leads to the magnetic Hamiltonian:

$$H_m = \sum_{\boldsymbol{k}} \hbar\epsilon_{\boldsymbol{k}} b^\dagger_{\boldsymbol{k}} b_{\boldsymbol{k}}, \tag{17}$$

where $\epsilon_{\boldsymbol{k}} = \gamma B + J_s\boldsymbol{k}^2/\hbar$ is the magnon frequency dispersion relation and $b^\dagger_{\boldsymbol{k}}(b_{\boldsymbol{k}})$ are creation (annihilation) operators of a magnon with wave vector $\boldsymbol{k}$.

Analogously, the finite size of a sufficiently large system only affects phonons with wavelengths $\mathcal{O}(V^{1/3})$ and a small density of states. We may then expand $\boldsymbol{u}_i = N^{-1/2}\sum_{\boldsymbol{k}} e^{-i\boldsymbol{k}\cdot\boldsymbol{R}_i}\boldsymbol{u}_{\boldsymbol{k}}$, with

$$\boldsymbol{u}_{\boldsymbol{k}} = \sum_\lambda \sqrt{\frac{\hbar}{2m\omega_{\boldsymbol{k}\lambda}}}\hat{\boldsymbol{e}}_{\boldsymbol{k}\lambda}\left(a_{\boldsymbol{k}\lambda} + a^\dagger_{-\boldsymbol{k}\lambda}\right). \tag{18}$$

Here, $a^\dagger_{\boldsymbol{k}\lambda}(a_{\boldsymbol{k}\lambda})$ creates (annihilates) a phonon with momentum $\boldsymbol{k}$, polarization vector $\hat{\boldsymbol{e}}_{\boldsymbol{k}\lambda}$, and frequency $\omega_{\boldsymbol{k}\lambda}$, and Bose commutation relations $[a_{\boldsymbol{k}\lambda}, a^\dagger_{\boldsymbol{k}'\lambda'}] = \delta_{\boldsymbol{k}\boldsymbol{k}'}\delta_{\lambda\lambda'}$. An isotropic elastic solid supports three acoustic phonon branches: two degenerate transverse ($\lambda = \pm$) and one longitudinal ($\lambda = \parallel$) one, with $\omega_{\boldsymbol{k}\lambda} = c_\lambda k$, where the c_λ are the sound velocities. We choose a circular basis $\lambda = \pm$ for the transverse phonons [11,15,45] and express the momentum $\boldsymbol{k}$ in spherical coordinates, so that

$$\begin{aligned}\hat{\boldsymbol{e}}_{\boldsymbol{k}\pm} &= \frac{1}{\sqrt{2}}[\hat{\boldsymbol{e}}_x(\cos\theta_{\boldsymbol{k}}\cos\phi_{\boldsymbol{k}} \mp i\sin\phi_{\boldsymbol{k}}) \\ &\quad + \hat{\boldsymbol{e}}_y(\cos\theta_{\boldsymbol{k}}\sin\phi_{\boldsymbol{k}} \pm i\cos\phi_{\boldsymbol{k}}) - \hat{\boldsymbol{e}}_z\sin\theta_{\boldsymbol{k}}], \qquad (19a)\\ \hat{\boldsymbol{e}}_{\boldsymbol{k}\parallel} &= i[\hat{\boldsymbol{e}}_x\sin\theta_{\boldsymbol{k}}\cos\phi_{\boldsymbol{k}} + \hat{\boldsymbol{e}}_y\sin\theta_{\boldsymbol{k}}\sin\phi_{\boldsymbol{k}} + \hat{\boldsymbol{e}}_z\cos\theta_{\boldsymbol{k}}] \\ &= i\frac{\boldsymbol{k}}{k}. \qquad (19b)\end{aligned}$$

In this basis the phonon spin (8) is diagonal [11,15,45]:

$$\boldsymbol{L} = -\hbar\sum_{\boldsymbol{k}} \frac{\boldsymbol{k}}{k}(a^\dagger_{\boldsymbol{k}+}a_{\boldsymbol{k}+} - a^\dagger_{\boldsymbol{k}-}a_{\boldsymbol{k}-}), \tag{20}$$

where we dropped terms that have vanishing expectation values for noninteracting phonons. Analogous to photons, circularly polarized phonons with $\lambda = \pm$ carry one spin quantum $\mp\hbar$ parallel to their wave vector that is carried exclusively by transverse phonons. Mentink *et al.* [13] report that only longitudinal phonons contribute to the electron-phonon spin transfer. This is not a contradiction, because they define phonon angular momentum different from Eq. (8) as adhered to in most papers [11,15,45]. On the other hand, that definition appears similar to the field (or pseudo) angular momentum introduced independently by Nakane and Kohno [18].

The leading one-phonon/one- and two-magnon contributions to the magnetoelastic Hamiltonian (12) read in momentum space

$$\begin{aligned}H_{mp} &= \sum_{\boldsymbol{k}}(\boldsymbol{\Gamma}_{\boldsymbol{k}}b_{\boldsymbol{k}} + \boldsymbol{\Gamma}^*_{-\boldsymbol{k}}b^\dagger_{-\boldsymbol{k}})\cdot\boldsymbol{u}_{-\boldsymbol{k}} \\ &\quad + \frac{1}{\sqrt{N}}\sum_{\boldsymbol{k}\boldsymbol{k}'}\Big(\boldsymbol{U}_{\boldsymbol{k},\boldsymbol{k}'}\cdot\boldsymbol{u}_{\boldsymbol{k}-\boldsymbol{k}'}b^\dagger_{\boldsymbol{k}}\hat{b}_{\boldsymbol{k}'} \\ &\quad + \frac{1}{2}\boldsymbol{V}_{\boldsymbol{k},\boldsymbol{k}'}\cdot\boldsymbol{u}_{-\boldsymbol{k}-\boldsymbol{k}'}b_{\boldsymbol{k}}b_{\boldsymbol{k}'} + \frac{1}{2}\boldsymbol{V}^*_{\boldsymbol{k},\boldsymbol{k}'}\cdot\boldsymbol{u}_{\boldsymbol{k}+\boldsymbol{k}'}b^\dagger_{\boldsymbol{k}}b^\dagger_{\boldsymbol{k}'}\Big), \qquad (21)\end{aligned}$$

with interaction vertices

$$\begin{aligned}\boldsymbol{\Gamma}_{\boldsymbol{k}} &= -\frac{iB_\perp}{\sqrt{2S}}[(\hat{\boldsymbol{e}}_x - i\hat{\boldsymbol{e}}_y)k^z + \hat{\boldsymbol{e}}_z(k^x - ik^y)], \qquad (22a)\\ \boldsymbol{U}_{\boldsymbol{k}+\boldsymbol{q},\boldsymbol{k}} &= \frac{iB_\parallel}{S}(\hat{\boldsymbol{e}}_x q^x + \hat{\boldsymbol{e}}_y q^y - 2\hat{\boldsymbol{e}}_z q^z) \\ &\quad + \frac{2iA_\parallel}{S}\sum_\alpha \hat{\boldsymbol{e}}_\alpha(k^\alpha + q^\alpha)k^\alpha q^\alpha, \qquad (22b)\\ \boldsymbol{V}_{\boldsymbol{k}+\boldsymbol{q},-\boldsymbol{k}} &= -\frac{iB_\parallel}{S}(\hat{\boldsymbol{e}}_x q^x - \hat{\boldsymbol{e}}_y q^y) - \frac{B_\perp}{S}(\hat{\boldsymbol{e}}_x q^y + \hat{\boldsymbol{e}}_y q^x). \qquad (22c)\end{aligned}$$

The first line of the magnetoelastic Hamiltonian (21) describes the hybridization of magnons and phonons or magnon polaron [5], while the second and third line are, respectively, magnon-number conserving Cherenkov scattering and magnon-number nonconserving confluence processes [28] as illustrated by Fig. 3. We disregard the weak two-phonon one-magnon scattering processes [7]. Angular momentum is transferred between the magnetic order and the lattice by the magnon-number nonconserving hybridization and confluence processes, while magnon-number conserving

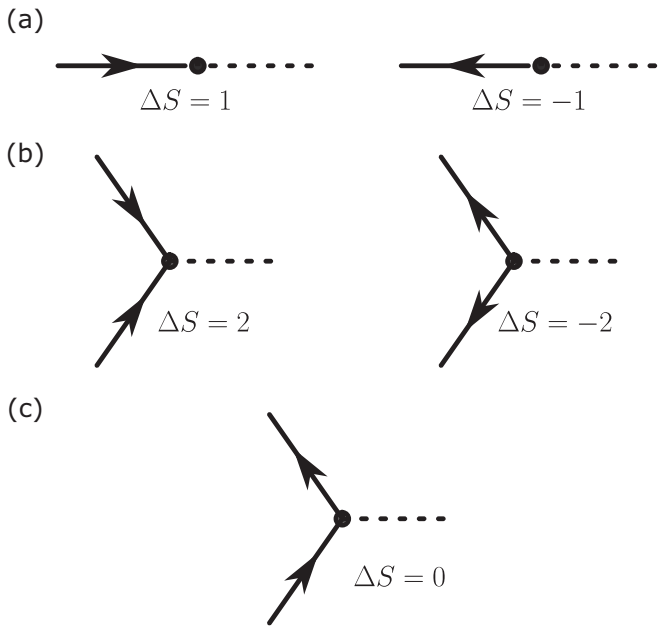

FIG. 3. Diagrams of the leading magnon-phonon scattering processes in Eq. (21), with corresponding change of electron spin ΔS. Solid, directed lines denote magnons and dashed lines phonons. (a) Magnon-phonon hybridization, (b) magnon-number nonconserving confluence processes, and (c) magnon-number conserving Cherenkov scattering.

scatterings transfer energy only. Energy conservation requires that phonons have frequencies larger than γB ($2\gamma B$), i.e., in the GHz range, in order to participate resonantly (by confluence) to the spin transfer. The applied magnetic field is an important control parameter since above the critical value

$$B_{c,\lambda} = \frac{\hbar c_\lambda^2}{4\gamma J_s} \tag{23}$$

hybridization and confluence processes are forbidden for phonons with polarization λ. For $B_{\rm ext} > B_{c,\perp}, B_{c,\parallel}$ other spin transfer mechanisms must be invoked, such as interface/surface [20] or higher order magnon-phonon scattering [7].

A. Kinetic equations

Treating the magnon-phonon interaction Hamiltonian (21) by Fermi's golden rule leads to rate equations for the bulk magnon and phonon distribution functions $n_{\boldsymbol{k}} = \langle b_{\boldsymbol{k}}^\dagger b_{\boldsymbol{k}}\rangle$ and $N_{\boldsymbol{k}\lambda} = \langle a_{\boldsymbol{k}\lambda}^\dagger a_{\boldsymbol{k}\lambda}\rangle$ [28]:

$$\begin{aligned}\dot{n}_{\boldsymbol{k}} =& \sum_\lambda \frac{\pi|\hat{\boldsymbol{e}}_{\boldsymbol{k}\lambda}^* \cdot \boldsymbol{\Gamma}_{\boldsymbol{k}}|^2}{m\hbar\omega_{\boldsymbol{k}\lambda}}\delta(\epsilon_{\boldsymbol{k}} - \omega_{\boldsymbol{k}\lambda})(N_{\boldsymbol{k}\lambda} - n_{\boldsymbol{k}}) \\ &+ \frac{1}{N}\sum_{\boldsymbol{k}'\boldsymbol{q}\lambda}\delta_{\boldsymbol{k}-\boldsymbol{k}',\boldsymbol{q}}\frac{\pi|\hat{\boldsymbol{e}}_{\boldsymbol{q}\lambda}\cdot\boldsymbol{U}_{\boldsymbol{k},\boldsymbol{k}'}|^2}{m\hbar\omega_{\boldsymbol{q}\lambda}}\delta(\epsilon_{\boldsymbol{k}} - \epsilon_{\boldsymbol{k}'} - \omega_{\boldsymbol{q}\lambda}) \\ &\times [(1+n_{\boldsymbol{k}})n_{\boldsymbol{k}'}N_{\boldsymbol{q}\lambda} - n_{\boldsymbol{k}}(1+n_{\boldsymbol{k}'})(1+N_{\boldsymbol{q}\lambda})] \\ &+ \frac{1}{N}\sum_{\boldsymbol{k}'\boldsymbol{q}\lambda}\delta_{\boldsymbol{k}-\boldsymbol{k}',\boldsymbol{q}}\frac{\pi|\hat{\boldsymbol{e}}_{\boldsymbol{q}\lambda}\cdot\boldsymbol{U}_{\boldsymbol{k},\boldsymbol{k}'}|^2}{m\hbar\omega_{\boldsymbol{q}\lambda}}\delta(\epsilon_{\boldsymbol{k}} - \epsilon_{\boldsymbol{k}'} + \omega_{\boldsymbol{q}\lambda}) \\ &\times [(1+n_{\boldsymbol{k}})n_{\boldsymbol{k}'}(1+N_{-\boldsymbol{q}\lambda}) - n_{\boldsymbol{k}}(1+n_{\boldsymbol{k}'})N_{-\boldsymbol{q}\lambda}] \\ &+ \frac{1}{N}\sum_{\boldsymbol{k}'\boldsymbol{q}\lambda}\delta_{\boldsymbol{k}+\boldsymbol{k}',\boldsymbol{q}}\frac{\pi|\hat{\boldsymbol{e}}_{\boldsymbol{q}\lambda}^*\cdot\boldsymbol{V}_{\boldsymbol{k},\boldsymbol{k}'}|^2}{m\hbar\omega_{\boldsymbol{q}\lambda}}\delta(\epsilon_{\boldsymbol{k}} + \epsilon_{\boldsymbol{k}'} - \omega_{\boldsymbol{q}\lambda}) \\ &\times [(1+n_{\boldsymbol{k}})(1+n_{\boldsymbol{k}'})N_{\boldsymbol{q}\lambda} - n_{\boldsymbol{k}}n_{\boldsymbol{k}'}(1+N_{\boldsymbol{q}\lambda})],\end{aligned} \tag{24}$$

and

$$\begin{aligned}\dot{N}_{\boldsymbol{q}\lambda} =& \frac{\pi|\hat{\boldsymbol{e}}_{\boldsymbol{q}\lambda}^*\cdot\boldsymbol{\Gamma}_{\boldsymbol{q}}|^2}{m\hbar\omega_{\boldsymbol{q}\lambda}}\delta(\epsilon_{\boldsymbol{q}} - \omega_{\boldsymbol{q}\lambda})(n_{\boldsymbol{q}} - N_{\boldsymbol{q}\lambda}) \\ &+ \frac{1}{N}\sum_{\boldsymbol{k}\boldsymbol{k}'}\delta_{\boldsymbol{k}-\boldsymbol{k}',\boldsymbol{q}}\frac{\pi|\hat{\boldsymbol{e}}_{\boldsymbol{q}\lambda}\cdot\boldsymbol{U}_{\boldsymbol{k},\boldsymbol{k}'}|^2}{m\hbar\omega_{\boldsymbol{q}\lambda}}\delta(\epsilon_{\boldsymbol{k}} - \epsilon_{\boldsymbol{k}'} - \omega_{\boldsymbol{q}\lambda}) \\ &\times [n_{\boldsymbol{k}}(1+n_{\boldsymbol{k}'})(1+N_{\boldsymbol{q}\lambda}) - (1+n_{\boldsymbol{k}})n_{\boldsymbol{k}'}N_{\boldsymbol{q}\lambda}] \\ &+ \frac{1}{N}\sum_{\boldsymbol{k}\boldsymbol{k}'}\delta_{\boldsymbol{k}+\boldsymbol{k}',\boldsymbol{q}}\frac{\pi|\hat{\boldsymbol{e}}_{\boldsymbol{q}\lambda}^*\cdot\boldsymbol{V}_{\boldsymbol{k},\boldsymbol{k}'}|^2}{2m\hbar\omega_{\boldsymbol{q}\lambda}}\delta(\epsilon_{\boldsymbol{k}} + \epsilon_{\boldsymbol{k}'} - \omega_{\boldsymbol{q}\lambda}) \\ &\times [n_{\boldsymbol{k}}n_{\boldsymbol{k}'}(1+N_{\boldsymbol{q}\lambda}) - (1+n_{\boldsymbol{k}})(1+n_{\boldsymbol{k}'})N_{\boldsymbol{q}\lambda}].\end{aligned} \tag{25}$$

The first term on the right-hand side of both Eqs. (24) and (25) is caused by the direct magnon-phonon conversion process in Fig. 3(a) that gives rise to magnetoelastic waves (magnon polarons) [5,46]. It diverges because perturbation theory breaks down at the crossing of magnon and phonon modes. The singularity can be removed by choosing a basis that diagonalizes the Hamiltonian [47]. Here we regularize it with a finite broadening [6] that is larger than the magnon-polaron gap, which leads to well-behaved integrated quantities such as energy, momentum, and spin densities.

B. Linear response

We capture the dynamics of energy and spin relaxation in linear response to weak perturbations, assuming that magnons and phonons stay close to a common thermal equilibrium at temperature T. The spin-lattice interaction transfers both energy and angular momentum which changes magnon and phonon energy

$$\delta E_m(t) = \frac{1}{V}\sum_{\boldsymbol{k}}\hbar\epsilon_{\boldsymbol{k}}\left[n_{\boldsymbol{k}}(t) - f_B\left(\frac{\hbar\epsilon_{\boldsymbol{k}}}{k_BT}\right)\right], \tag{26a}$$

$$\delta E_\lambda(t) = \frac{1}{V}\sum_{\boldsymbol{k}}\hbar\omega_{\boldsymbol{k}\lambda}\left[N_{\boldsymbol{k}\lambda}(t) - f_B\left(\frac{\hbar\omega_{\boldsymbol{k}\lambda}}{k_BT}\right)\right], \tag{26b}$$

as well as spin densities

$$\delta s(t) = \frac{\hbar}{V}\sum_{\boldsymbol{k}}\left[n_{\boldsymbol{k}}(t) - f_B\left(\frac{\hbar\epsilon_{\boldsymbol{k}}}{k_BT}\right)\right], \tag{27a}$$

$$\delta l(t) = \frac{\langle L^z(t)\rangle}{V} = -\frac{\hbar}{V}\sum_{\boldsymbol{k}}\frac{k^z}{k}[N_{k+}(t) - N_{k-}(t)], \tag{27b}$$

where $f_B(x) = 1/(e^x - 1)$ is the Bose distribution function. Since a precessing magnetic moment can inject a transverse, circularly polarized momentum current into an adjacent nonmagnetic insulator [20] we also consider transverse phonon momentum densities

$$\rho_\pm(t) = \frac{1}{V}\sum_{\boldsymbol{k}}\hbar k^z N_{k\pm}(t), \tag{28}$$

with $\rho_+ = -\rho_-$ at equilibrium. In a driven system $\delta\rho = \rho_+ - \rho_-$ can be finite as can be seen from the interaction vertex between magnons and transverse phonons in equations (24) and (25):

$$|\hat{\boldsymbol{e}}^*_{\boldsymbol{k}\pm}\cdot\boldsymbol{\Gamma}|^2 = \frac{B_\perp^2 k^2}{4S}(\cos^2\theta_{\boldsymbol{k}} - \sin^2\theta_{\boldsymbol{k}} \mp \cos\theta_{\boldsymbol{k}})^2. \tag{29}$$

For phonons propagating along $\pm\hat{\boldsymbol{e}}_z$, i.e., with $\cos\theta_{\boldsymbol{k}} = \pm 1$, this expression is only finite for polarization direction $\lambda = \mp$. Hence, magnons couple to $\lambda = +$ ($\lambda = -$) phonons traveling in the $-\hat{\boldsymbol{e}}_z$ ($+\hat{\boldsymbol{e}}_z$) direction. An imbalance in the magnon distribution thus creates transverse phonon polarizations $\delta\rho$ and a finite phonon spin polarization (27b).

The coupled kinetic equations (24) and (25) can be simplified by assuming that magnon-magnon and phonon-phonon interactions thermalize the distributions to a quasiequilibrium form that can be parametrized by slowly varying variables conjugate to the macroscopic observables of interest [6,48], i.e., the energy and spin densities given in Eqs. (26a) and (27a), respectively. These conjugate variables are a temperature deviation $\delta T_m(t)$ and a magnon chemical potential $\mu(t)$ [48], such that

$$n_{\boldsymbol{k}}(t) = f_B\left(\frac{\hbar\epsilon_{\boldsymbol{k}} - \mu(t)}{k_B(T + \delta T_m(t))}\right). \tag{30}$$

This parametrization of the magnon distribution is accurate for thermal magnons when the number-conserving exchange interaction is the dominant scattering mechanism, which is usually the case in magnetic insulators [28,48].

A parametrization such as Eq. (30) of the phonon distribution fails because a phonon chemical potential does not lead to a finite phonon spin polarization $\delta\rho$ because the angular dependence, $k_z \propto \cos\theta_{\boldsymbol{k}}$ in Eq. (28), averages to zero when the distribution $N_{\boldsymbol{k}\pm}$ is isotropic in momentum space. We therefore focus on the leading anisotropic term, which is a Bose distribution rigidly shifted by a polarization-dependent phonon drift velocity v_λ:

$$N_{\boldsymbol{k}\lambda}(t) = f_B\left(\frac{\hbar\omega_{\boldsymbol{k}\lambda} - \hbar v_\lambda(t)k^z}{k_B(T + \delta T_\lambda(t))}\right). \tag{31}$$

Because the transverse phonon modes are degenerate, we set $\delta T_+(t) = \delta T_-(t) \equiv \delta T_\perp(t)$ without loss of generality, but we allow for different temperatures of longitudinal and transverse phonons, $\delta T_\parallel(t)$ and $\delta T_\perp(t)$, and associated energy densities. Global linear momentum conservation requires $v_+(t) = -v_-(t) \equiv v(t)$ and $v_\parallel(t) = 0$. Just as for the magnon distribution function (30), the parametrization (31) of the phonon distribution function contains some tacit assumptions about the relative importance of different scattering mechanisms: In particular, it should be applicable when polarization- and momentum-conserving phonon-phonon scattering dominates over the nonconserving scattering mechanisms. In YIG, the acoustic quality is much better than the magnetic one [5], which supports our shifted-distribution ansatz (31). Also, a finite drift velocity v implies existence of a phonon current on relatively large time scales, which requires a system size $\sim V^{1/3}$ larger than the phonon relaxation length.

The response to leading order in the nonequilibrium parameters reads

$$\delta E_m(t) = -\frac{1}{V}\sum_{\boldsymbol{k}} f_B'\left(\frac{\hbar\epsilon_{\boldsymbol{k}}}{k_BT}\right)\hbar\epsilon_{\boldsymbol{k}}\left(\frac{\hbar\epsilon_{\boldsymbol{k}}}{k_BT}\frac{\delta T_m(t)}{T} + \frac{\mu(t)}{k_BT}\right), \tag{32a}$$

$$\delta E_\lambda(t) = -\frac{1}{V}\sum_{\boldsymbol{k}} f_B'\left(\frac{\hbar\omega_{\boldsymbol{k}\lambda}}{k_BT}\right)\hbar\omega_{\boldsymbol{k}\lambda}\frac{\hbar\omega_{\boldsymbol{k}\lambda}}{k_BT}\frac{\delta T_\lambda(t)}{T}, \tag{32b}$$

$$\delta s(t) = -\frac{\hbar}{V}\sum_{\boldsymbol{k}} f_B'\left(\frac{\hbar\epsilon_{\boldsymbol{k}}}{k_BT}\right)\left(\frac{\hbar\epsilon_{\boldsymbol{k}}}{k_BT}\frac{\delta T_m(t)}{T} + \frac{\mu(t)}{k_BT}\right), \tag{32c}$$

$$\delta\rho(t) = -\frac{2\hbar}{V}\sum_{\boldsymbol{k}} f_B'\left(\frac{\hbar\omega_{\boldsymbol{k}\perp}}{k_BT}\right)(k^z)^2\frac{\hbar v(t)}{k_BT}, \tag{32d}$$

where $f_B'(x) = \partial f_B(x)/\partial x$, and the nonequilibrium phonon spin density is

$$\delta l(t) = \frac{2\hbar}{V}\sum_{\boldsymbol{k}} f_B'\left(\frac{\hbar\omega_{\boldsymbol{k}\perp}}{k_BT}\right)\frac{(k^z)^2}{k}\frac{\hbar v(t)}{k_BT}. \tag{33}$$

According to Eq. (7), the angular momentum of the rigid body rotation around a principal axis of the tensor of inertia is $I\Omega^z(t) = V[\delta j_0 + \delta s(t) - \delta l(t)]$, where δj_0 is an angular momentum density injected by external torques.

The linear response can be summarized by

$$\partial_t\begin{pmatrix}\delta E_m(t)/k_BT\\ \delta E_\perp(t)/k_BT\\ \delta E_\parallel(t)/k_BT\\ \delta s(t)/\hbar\\ c_\perp\delta\rho(t)/k_BT\end{pmatrix} = -\begin{pmatrix}\Gamma_\perp+\Gamma_\parallel & -\Gamma_\perp & -\Gamma_\parallel & -\Gamma_{\perp\mu}-\Gamma_{\parallel\mu} & -\Gamma_{\perp v}\\ -\Gamma_\perp & \Gamma_\perp & 0 & \Gamma_{\perp\mu} & \Gamma_{\perp v}\\ -\Gamma_\parallel & 0 & \Gamma_\parallel & \Gamma_{\parallel\mu} & 0\\ -\Gamma_{\perp\mu}-\Gamma_{\parallel\mu} & \Gamma_{\perp\mu} & \Gamma_{\parallel\mu} & \Gamma_\mu & \Gamma_{v\mu}\\ -\Gamma_{\perp v} & \Gamma_{\perp v} & 0 & \Gamma_{v\mu} & \Gamma_v\end{pmatrix}\begin{pmatrix}\delta T_m(t)/T\\ \delta T_\perp(t)/T\\ \delta T_\parallel(t)/T\\ \mu(t)/k_BT\\ v(t)/c_\perp\end{pmatrix}, \tag{34}$$

where $\delta E_\perp = \delta E_+ + \delta E_-$ is the change in the transverse phonon energy density. The Onsager-reciprocal relaxation rates $\Gamma_{\alpha\beta}$ from Eqs. (24) and (25) are listed in Appendix C.

In the following, we discuss the solutions for the material parameters of yttrium-iron garnet in Table I. We discuss three scenarios: (i) heating, (ii) parametric pumping by microwaves, and (iii) optical spin injection. First, we consider the scenario in which energy injected into the lattice, e.g., by a femtosecond laser pulse at an optical phonon resonance, relaxes very quickly to a distribution of the form (31), which subsequently releases energy to the magnetic system. In this case there is no angular momentum transfer from the environment and $\delta j_0 = 0$. Figure 4 shows the calculated dynamics when the magnetic order is perturbed by a sudden increase of the

TABLE I. Magnetic and elastic material parameters of yttrium-iron garnet, adopted from Refs. [7,28,48–50]. If not indicated otherwise, the parameters are measured at room temperature.

	Symbol	Value	Unit
lattice constant	a	12.376	Å
effective spin per unit cell for $T \lesssim 50$ K	S	20	
exchange stiffness constant	J_s	8.458×10^{-40}	J m^2
g factor	g	2	
mass per unit cell	m	9.800×10^{-24}	kg
longitudinal sound velocity	$c_\parallel$	7209	m s^{-1}
transverse sound velocity	$c_\perp$	3843	m s^{-1}
longitudinal critical field	$B_{c,\parallel}$	9.21	T
transverse critical field	$B_{c,\perp}$	2.62	T
magnetic Grüneisen parameter	Γ_m	−3.2	
diagonal magnetoelastic constant	$B_\parallel$	6.597×10^{-22}	J
off-diagonal magnetoelastic constant	$B_\perp$	1.319×10^{-21}	J
exchange magnetoelastic constant	$A_\parallel$	-8.120×10^{-38}	J m^2

phonon temperature $\delta T_\parallel(0) = \delta T_\perp(0)$. Parallel microwave pumping is the nonlinear process in which a microwave magnetic field parallel to the magnetization parametrically excites the Kittel mode above a certain threshold intensity. In contrast to the (linear) ferromagnetic resonance, the linearly polarized radiation does not inject angular momentum into the magnet, so also in this case $\delta j_0 = 0$. The angular momentum needed to excite the magnetization is therefore provided only by the lattice. We assume that the pumped magnons thermalize quickly to a distribution with increased temperature and finite magnon chemical potential, while the lattice is initially in equilibrium and plot the results in Fig. 5. The third scenario addresses the direct injection of angular momentum into the phonons. This can be achieved by exposing the magnet to circularly polarized light that couples only to phonons with a certain spin polarization, or by phonon spin pumping from a thin film of another magnet attached to the system [20]. Since the phonon spin is supplied by the external environment in this case, we have $\delta j_0 = \delta l(t = 0)$, while the magnons are initially in equilibrium. The response to such an external torque is plotted in Fig. 6.

The cases (i) and (ii) share many features. Figures 4(a) and 5(a) show that the energy relaxes in two stages: First, the longitudinal-phonon and magnon temperatures converge, after which they both equilibrate with the transverse-phonon temperature. The longitudinal phonons and the magnons equilibrate faster than the transverse phonons, because the specific heat of the former is an order of magnitude smaller than that of the latter. In parallel, the magnetoelastic coupling builds up transient, counterpropagating currents of the two circular phonon modes, i.e., a phononic spin, on a time scale similar to the magnon chemical potential or spin accumulation, see Figs. 4(b) and 5(b). The phonon spin density generated by phonon heating is typically an order of magnitude smaller than the magnon spin. The induced rigid rotation in Fig. 4(c) is therefore mainly a magnonic effect. However, when the system is excited by pumping the magnons, the phonon spin transiently dominates the magnon contribution, see Fig. 5(c). The angular velocity Ω^z temporarily changes sign, i.e., the body rotates in the opposite direction, seemingly breaking the angular conservation law. After the magnon-dominated

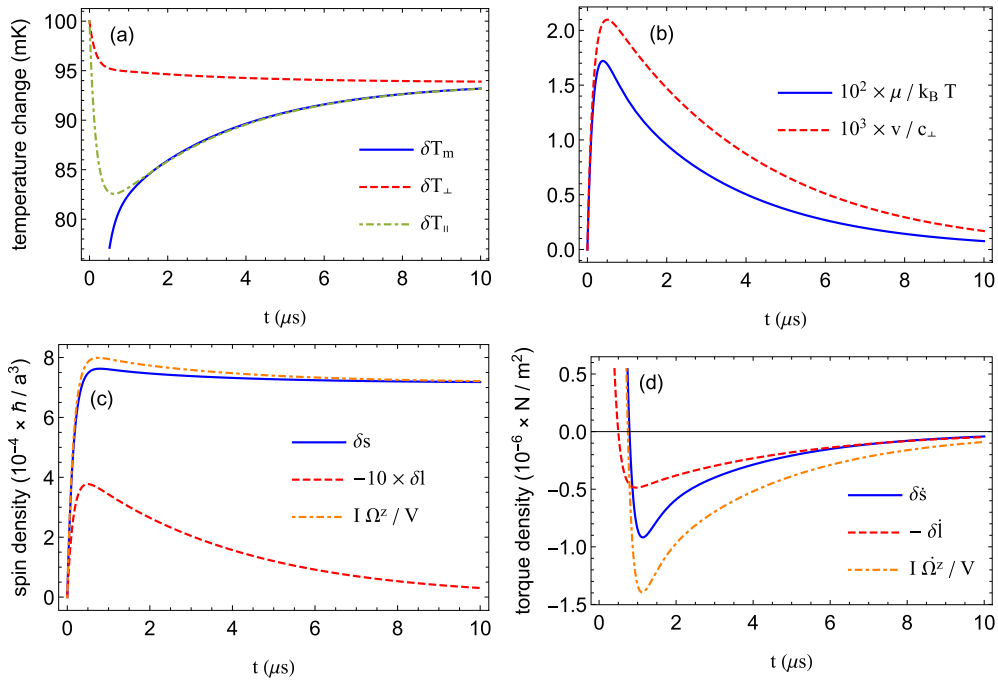

FIG. 4. Nonequilibrium dynamics of (a) magnon and phonon temperatures, (b) magnon chemical potential and phonon drift velocity, (c) spin densities, and (d) torque densities of magnons, phonons, and rigid rotation, for heating initial conditions $\delta T_\perp(t = 0) = \delta T_\parallel(t = 0) = 1$ K, and $\delta T_m(t = 0) = \mu(t = 0) = v(t = 0) = 0$. Temperature and external magnetic field are $T = 10$ K and $B = 1$ T.

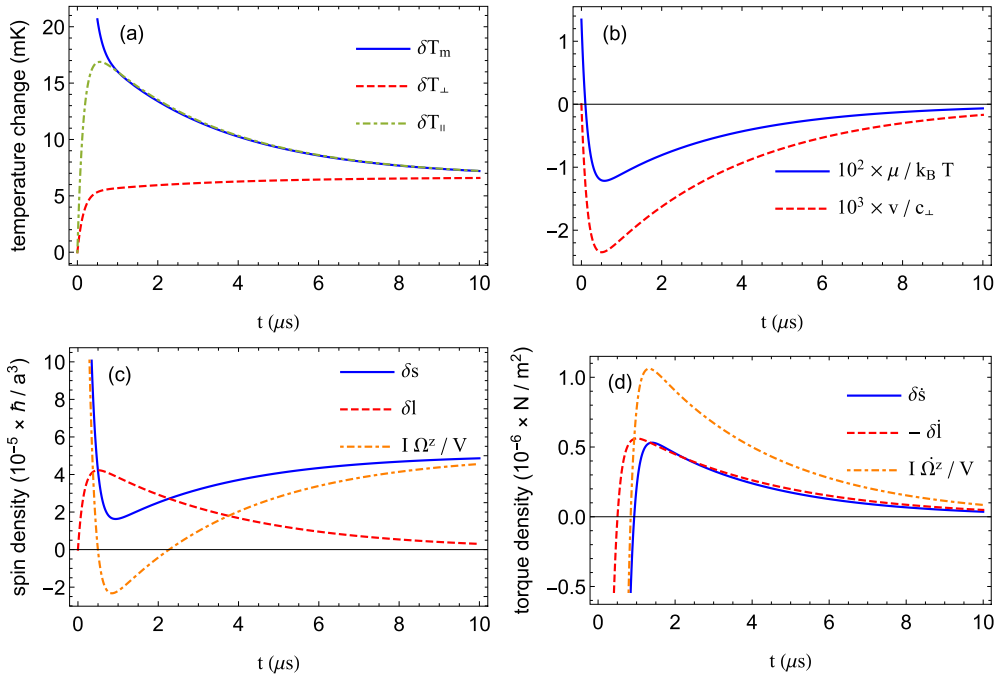

FIG. 5. Nonequilibrium dynamics of (a) magnon and phonon temperatures, (b) magnon chemical potential and phonon drift velocity, (c) spin densities, and (d) torque densities of magnons, phonons, and rigid rotation, with initial conditions $\delta T_m(t=0) = 1\,\mathrm{K}$, $\mu(t=0) = 0.1 \times \hbar\gamma B$, and $\delta T_\perp(t=0) = \delta T_\parallel(t=0) = v(t=0) = 0$, corresponding to magnon pumping, e.g., by applying a parallel parametric pumping field. Temperature and external magnetic field are $T = 10\,\mathrm{K}$ and $B = 1\,\mathrm{T}$.

first microsecond, the torques exerted by both phonons and magnons in Figs. 4(d) and 5(d) are very similar.

Figure 6 sketches the even more dramatic effect when the injected phonons initially carry a spin without excess energy, which means that the system at large times must relax to the initial temperature T. However, spin may be transferred from the phonons to the magnons, which heats the magnons and endows them with a finite chemical potential, see

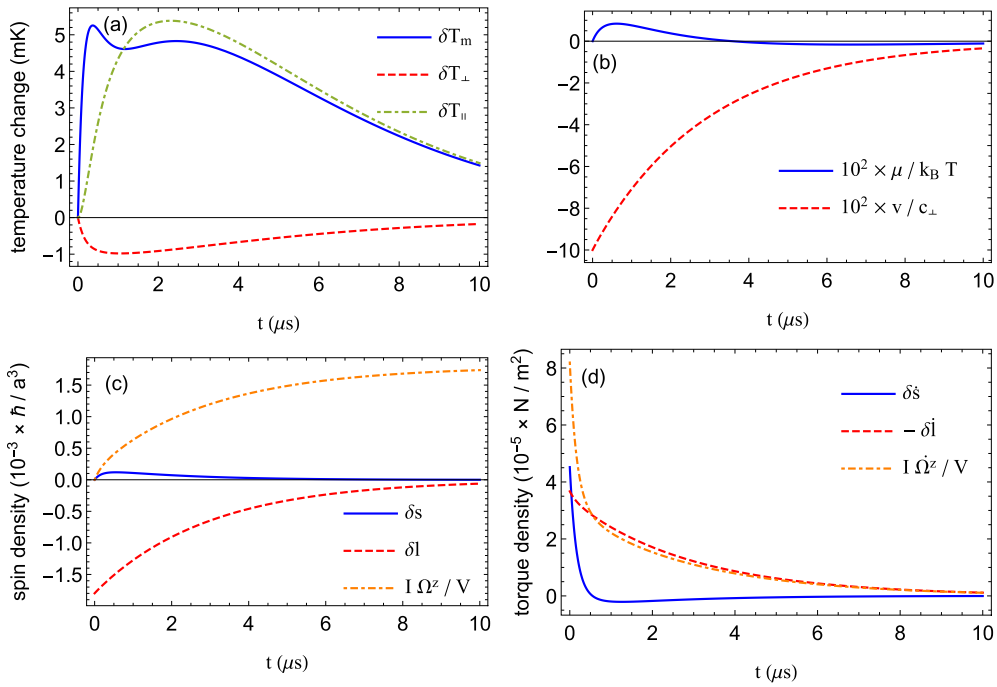

FIG. 6. Nonequilibrium dynamics of (a) magnon and phonon temperatures, (b) magnon chemical potential and phonon drift velocity, (c) spin densities, and (d) torque densities of magnons, phonons, and rigid rotation, with initial conditions $v(t=0) = -0.1 \times c_\perp$, and $\delta T_\perp(t=0) = \delta T_\parallel(t=0) = \delta T_m(t=0) = \mu(t=0) = 0$. corresponding to a finite phonon spin. Temperature and external magnetic field are $T = 10\,\mathrm{K}$ and $B = 1\,\mathrm{T}$.

Figs. 6(a)–6(c), which is only possible by transient cooling of the transverse phonons. Actually only a small fraction of the spin is transferred from the phonons to the magnons in Fig. 6(c): The loss of phonon spin is accommodated by the rigid rotation of the entire magnet. The overall torque in Fig. 6(d) is dominated by the phonons at almost all times.

IV. DISCUSSION AND CONCLUSIONS

We present a microscopic theory of spin-lattice interactions and angular momentum conservation in magnetic insulators. After separating the mechanical degrees of freedom into rigid-body and internal vibrations, we find that also phonons carry internal angular momentum. We derive equations of motion for the spin, rigid-body, and phonon spin operators that govern the Einstein-de Haas and Barnett effects, and show that the torque generated by spin-lattice interactions drives both the rigid-body rotation and the phonon spin. In the long-wavelength limit, we recover the phenomenological theory of magnetoelasticity.

We apply the formalism to a linear response analysis of a levitated magnet that is large enough that surface effects can be disregarded but small enough that rotations are observable. In contrast to the magnon chemical potential or accumulation, the phonon chemical potential does not couple to the total rotation. It is rather an internal phonon current that governs the phonon contribution to the Einstein-de Haas effect. Depending on the driving protocol, the transient Einstein-de Haas dynamics can involve a change in the sense of rotation. When the system is not levitated but fixed, e.g., on a substrate, the torques exerted by the magnon and phonon spins on the sample are in principle measurable [51–53]. Brillouin light scattering [16] can resolve the phonon spin; our prediction of a momentum imbalance between the two circularly polarized phonon modes should therefore also be experimentally accessible.

Several assumptions and approximations imply that the present results are valid for a limited temperature and size of the system. The adoption of the magnetoelastic limit implies that temperatures should not exceed the frequencies for which a continuum mechanics and magnetism holds, roughly $T < 100\,\mathrm{K}$. The decoupling of internal phonon modes from the total rotation introduces errors that we estimate to vanish when the number of spins is much larger than unity which is not very restrictive. More drastic is the assumption that the phonon relaxation length should be much smaller than the systems size, in order to allow the flow of transient phonon spin currents. This is a material specific and temperature dependent parameter that is not well known. When the phonon relaxation length is much larger than the particle size, a phonon spin does not build up, strongly suppressing the phonon contribution to the Einstein-de Haas effect. For materials with extremely low acoustic attenuation such as YIG, the phonon propagation length at GHz frequencies can be centimeters. Thermal phonons at not too low temperatures are more strongly scattered, which leads us to believe that YIG spheres that can be fabricated for diameters $\gtrsim$0.5 mm are suitable model systems to test our predictions. The size estimates for other materials can be substantially smaller, however. For particles larger than the phonon relaxation length, the ratio between predicted torques and total volume is predicted to be constant as long as the excitation is more or less homogeneous.

Our treatment of angular momentum transfer in spin-lattice interactions should be useful in the study of a variety of problems. Of particular interest would be the application to the magnetic nanosystems like cantilevers [51–53] and nanoparticles in polymer cavities [54] or levitated in traps [22–25]. It could also be extended to study the role of the phonon spin in transport phenomena like the spin Seebeck effect [1]. Moreover, the microscopic spin-lattice Hamiltonian that we proposed could be used to extend computations of magnon-phonon interactions [7] into the high-temperature regime where magnetoelastic theory is no longer valid and to determine material constants from *ab initio* computations. Another extension of the formalism would allow addressing finite-size corrections, quantum effects, and time scales at which rigid-body and internal phonon dynamics cannot be separated.

ACKNOWLEDGMENTS

This work is supported by the European Research Council via Consolidator Grant No. 725509 SPINBEYOND and JSPS KAKENHI Grant No. 19H006450. R.A.D. is a member of the D-ITP consortium, a program of the Netherlands Organisation for Scientific Research (NWO) that is funded by the Dutch Ministry of Education, Culture and Science (OCW). This work is also part of the normal research program of NWO. This research was supported in part by the National Science Foundation under Grant No. NSF PHY-1748958.

APPENDIX A: TOTAL ANGULAR MOMENTUM CONSERVATION

In terms of the three Euler angles ϕ, θ, and χ as defined in Eq. (3) the body-fixed total angular momentum operator reads (see, e.g., Refs. [40,41] for details)

$$\boldsymbol{J} = \frac{\hbar}{i}\begin{pmatrix} \partial_\chi \\ \frac{\sin\chi}{\cos\theta}\partial_\phi + \cos\chi\,\partial_\theta + \tan\theta\sin\chi\,\partial_\chi \\ \frac{\cos\chi}{\cos\theta}\partial_\phi - \sin\chi\,\partial_\theta + \tan\theta\cos\chi\,\partial_\chi \end{pmatrix}. \tag{A1}$$

In the laboratory frame

$$\boldsymbol{J}_{\mathrm{lab}} = \mathcal{R}(\phi,\theta,\chi)\boldsymbol{J} \tag{A2}$$

$$= \frac{\hbar}{i}\begin{pmatrix} \cos\phi\tan\theta\,\partial_\phi - \sin\phi\,\partial_\theta + \frac{\cos\phi}{\cos\theta}\partial_\chi \\ \sin\phi\tan\theta\,\partial_\phi + \cos\phi\,\partial_\theta + \frac{\sin\phi}{\cos\theta}\partial_\chi \\ \partial_\phi \end{pmatrix}. \tag{A3}$$

These operators obey the commutation relations

$$[J^x, J^y] = -i\hbar J^z, \tag{A4}$$

$$\left[J^x_{\mathrm{lab}}, J^y_{\mathrm{lab}}\right] = i\hbar J^z_{\mathrm{lab}}, \tag{A5}$$

including their cyclic permutations. Also, $\boldsymbol{J}^2 = \boldsymbol{J}^2_{\mathrm{lab}}$, and

$$\left[\boldsymbol{J}^2_{\mathrm{lab}}, \boldsymbol{J}\right] = 0, \tag{A6}$$

$$\left[J^z_{\mathrm{lab}}, \boldsymbol{J}\right] = 0, \tag{A7}$$

whereas

$$[\boldsymbol{J}_{\rm lab}, U^\dagger H_S U] = i\hbar \sum_{i=1}^{N} [\mathcal{R}(\phi,\theta,\chi)\boldsymbol{S}_i] \times \gamma \boldsymbol{B} + i\hbar \mathcal{R}(\phi,\theta,\chi)\boldsymbol{\mathcal{T}}_{\rm ext}. \tag{A8}$$

Hence, in the absence of torques by an external magnetic field $\boldsymbol{B}$ or external mechanical forces, the absolute value $\boldsymbol{J}^2_{\rm lab}$ and the z component $J^z_{\rm lab}$ of the total angular momentum are conserved.

APPENDIX B: PHONON COMMUTATION RELATIONS

The commutator of the phonon displacement and position operators introduced in Eq. (9) is given by

$$\left[u_i^\alpha, \pi_j^\beta\right] = i\hbar\sqrt{\frac{m_j}{m_i}} \sum_{n=1}^{3N-6} f_n^\alpha(\boldsymbol{R}_i) f_m^\beta(\boldsymbol{R}_j) \tag{B1}$$

$$= i\hbar\left[\delta_{ij}\delta^{\alpha\beta} - \sqrt{\frac{m_j}{m_i}} \sum_{n\in\text{zero modes}} f_n^\alpha(\boldsymbol{R}_i) f_m^\beta(\boldsymbol{R}_j)\right], \tag{B2}$$

where we used the completeness relation $\sum_{n=1}^{3N} f_n^\alpha(\boldsymbol{R}_i) f_m^\beta(\boldsymbol{R}_j) = \delta_{ij}\delta^{\alpha\beta}$ for the combined phonon and rigid-body zero modes.

Explicit expressions for the 6 zero mode eigenfunctions of center-of-mass translation and rigid rotation must obey the translational and rotational invariance. The transformation $\boldsymbol{R}_i \to \boldsymbol{R}_i + \boldsymbol{a}$, where $\boldsymbol{a}$ is a constant vector, leaves the potential $V(\{\boldsymbol{r}_i\})$ invariant. Comparing to the definition (3) of the phonon eigenmode expansion in the body-fixed frame, we find the 3 (normalized) zero mode eigenfunctions of center-of-mass translation

$$\boldsymbol{f}_{{\rm CM},\mu}(\boldsymbol{R}_i) = \sqrt{\frac{m_i}{M}}\hat{\boldsymbol{e}}_\mu, \tag{B3}$$

where the $\hat{\boldsymbol{e}}_\mu$ with $\mu = 1,2,3$ are an arbitrary set of orthonormal basis vectors. Similarly, we obtain the 3 zero modes of rigid rotation by considering infinitesimal rotations $\boldsymbol{R}_i \to \boldsymbol{R}_i + \boldsymbol{\phi} \times \boldsymbol{R}_i$, with $|\boldsymbol{\phi}| \ll 1$, yielding

$$\boldsymbol{f}_{R,\mu}(\boldsymbol{R}_i) = \sqrt{\frac{m_i}{I_\mu}}\hat{\boldsymbol{n}}_\mu \times \boldsymbol{R}_i. \tag{B4}$$

Here the $\hat{\boldsymbol{n}}_\mu$ with $\mu = 1,2,3$ are the principal axes of the system in the body-fixed frame, and I_μ the corresponding principal moments of inertia. The commutator (B2) becomes

$$\left[u_i^\alpha, \pi_j^\beta\right] = i\hbar\left[\delta_{ij}\delta^{\alpha\beta} - \frac{m_j}{M}\delta^{\alpha\beta} - \sum_{\mu=1}^{3} \frac{m_j(\hat{\boldsymbol{n}}_\mu \times \boldsymbol{R}_i)^\alpha (\hat{\boldsymbol{n}}_\mu \times \boldsymbol{R}_j)^\beta}{I_\mu}\right]. \tag{B5}$$

We can estimate the order of magnitude of the corrections to the commutation relations by introducing a unit cell around each particle with volume $\Delta V = V/N$ and mass $m_i \approx \rho\Delta V$, where $\rho = M/V$ is the mass density. The maximum distance $\boldsymbol{R}_i$ of a particle from the origin is of the order $V^{1/3}$, so the moment of inertia $I_\mu \sim \rho V^{5/3}$. Hence

$$\frac{m_j}{M} \sim \frac{\rho\Delta V}{\rho V} = \frac{1}{N}, \tag{B6a}$$

$$\frac{m_j(\hat{\boldsymbol{n}}_\mu \times \boldsymbol{R}_i)^\alpha (\hat{\boldsymbol{n}}_\mu \times \boldsymbol{R}_j)^\beta}{I_\mu} \sim \frac{\rho\Delta V V^{2/3}}{\rho V^{5/3}} = \frac{1}{N}. \tag{B6b}$$

Therefore, the noncanonical corrections to the commutator (B2) scale with the inverse of the number of particles N in the system; hence the phonon operators (9) and (8) in the body-fixed frame can be treated as canonical whenever $N \gg 1$, so one has to worry about corrections only for small molecules.

APPENDIX C: LINEAR RESPONSE RELAXATION RATES

The linear response relaxation rates

$$\Gamma_{\alpha\beta} = \Gamma^{(1)}_{\alpha\beta} + \Gamma^{(2)}_{\alpha\beta}, \tag{C1}$$

where $\Gamma^{(1)}_{\alpha\beta}$ and $\Gamma^{(2)}_{\alpha\beta}$ are due to one-magnon one-phonon and two-magnon one-phonon processes, respectively, follow from inserting the ansätze (30) and (31) for the magnon and phonon distribution functions into the kinetic equations (24) and (25). Explicitly,

$$\Gamma^{(1)}_{\perp} = \frac{\pi\hbar}{mk_B^2T^2V}\sum_{\boldsymbol{k}} \omega_{\boldsymbol{k}\lambda}\delta_{\lambda,\perp}|\hat{\boldsymbol{e}}^*_{\boldsymbol{k}\lambda}\cdot\boldsymbol{\Gamma}_{\boldsymbol{k}}|^2\delta(\epsilon_{\boldsymbol{k}} - \omega_{\boldsymbol{k}\lambda})\left[1 + f_B\left(\frac{\hbar\epsilon_{\boldsymbol{k}}}{k_BT}\right)\right]f_B\left(\frac{\hbar\epsilon_{\boldsymbol{k}}}{k_BT}\right), \tag{C2a}$$

$$\Gamma^{(1)}_{\parallel} = \frac{\pi\hbar}{mk_B^2T^2V}\sum_{\boldsymbol{k}} \omega_{\boldsymbol{k}\lambda}\delta_{\lambda,\parallel}|\hat{\boldsymbol{e}}^*_{\boldsymbol{k}\lambda}\cdot\boldsymbol{\Gamma}_{\boldsymbol{k}}|^2\delta(\epsilon_{\boldsymbol{k}} - \omega_{\boldsymbol{k}\lambda})\left[1 + f_B\left(\frac{\hbar\epsilon_{\boldsymbol{k}}}{k_BT}\right)\right]f_B\left(\frac{\hbar\epsilon_{\boldsymbol{k}}}{k_BT}\right), \tag{C2b}$$

$$\Gamma^{(1)}_{v} = \frac{\pi\hbar c_\perp^2}{mk_B^2T^2V}\sum_{\boldsymbol{k}\lambda} \delta_{\lambda,\perp}\left(k^z\right)^2\frac{|\hat{\boldsymbol{e}}^*_{\boldsymbol{k}\lambda}\cdot\boldsymbol{\Gamma}_{\boldsymbol{k}}|^2}{\omega_{\boldsymbol{k}\lambda}}\delta(\epsilon_{\boldsymbol{k}} - \omega_{\boldsymbol{k}\lambda})\left[1 + f_B\left(\frac{\hbar\epsilon_{\boldsymbol{k}}}{k_BT}\right)\right]f_B\left(\frac{\hbar\epsilon_{\boldsymbol{k}}}{k_BT}\right), \tag{C2c}$$

$$\Gamma^{(1)}_{\perp v} = \frac{\pi\hbar c_\perp}{mk_B^2T^2V}\sum_{\boldsymbol{k}\lambda} \delta_{\lambda,\perp}\lambda k^z|\hat{\boldsymbol{e}}^*_{\boldsymbol{k}\lambda}\cdot\boldsymbol{\Gamma}_{\boldsymbol{k}}|^2\delta(\epsilon_{\boldsymbol{k}} - \omega_{\boldsymbol{k}\lambda})\left[1 + f_B\left(\frac{\hbar\epsilon_{\boldsymbol{k}}}{k_BT}\right)\right]f_B\left(\frac{\hbar\epsilon_{\boldsymbol{k}}}{k_BT}\right), \tag{C2d}$$

$$\Gamma^{(1)}_{\perp\mu} = -\frac{\pi}{mk_BTV}\sum_{\boldsymbol{k}\lambda} \delta_{\lambda,\perp}|\hat{\boldsymbol{e}}^*_{\boldsymbol{k}\lambda}\cdot\boldsymbol{\Gamma}_{\boldsymbol{k}}|^2\delta(\epsilon_{\boldsymbol{k}} - \omega_{\boldsymbol{k}\lambda})\left[1 + f_B\left(\frac{\hbar\epsilon_{\boldsymbol{k}}}{k_BT}\right)\right]f_B\left(\frac{\hbar\epsilon_{\boldsymbol{k}}}{k_BT}\right), \tag{C2e}$$

$$\Gamma^{(1)}_{\parallel\mu} = -\frac{\pi}{mk_BTV}\sum_{\boldsymbol{k}\lambda} \delta_{\lambda,\parallel}|\hat{\boldsymbol{e}}^*_{\boldsymbol{k}\lambda}\cdot\boldsymbol{\Gamma}_{\boldsymbol{k}}|^2\delta(\epsilon_{\boldsymbol{k}} - \omega_{\boldsymbol{k}\lambda})\left[1 + f_B\left(\frac{\hbar\epsilon_{\boldsymbol{k}}}{k_BT}\right)\right]f_B\left(\frac{\hbar\epsilon_{\boldsymbol{k}}}{k_BT}\right), \tag{C2f}$$

$$\Gamma^{(1)}_{v\mu} = -\frac{\pi c_\perp}{mk_BTV}\sum_{\boldsymbol{k}\lambda}\delta_{\lambda,\perp}\lambda k^z\frac{|\hat{\boldsymbol{e}}^*_{\boldsymbol{k}\lambda}\cdot\boldsymbol{\Gamma}_{\boldsymbol{k}}|^2}{\omega_{\boldsymbol{k}\lambda}}\delta(\epsilon_{\boldsymbol{k}}-\omega_{\boldsymbol{k}\lambda})\left[1+f_B\left(\frac{\hbar\epsilon_{\boldsymbol{k}}}{k_BT}\right)\right]f_B\left(\frac{\hbar\epsilon_{\boldsymbol{k}}}{k_BT}\right), \tag{C2g}$$

$$\Gamma^{(1)}_{\mu} = \frac{\pi}{\hbar mV}\sum_{\boldsymbol{k}\lambda}\frac{|\hat{\boldsymbol{e}}^*_{\boldsymbol{k}\lambda}\cdot\boldsymbol{\Gamma}_{\boldsymbol{k}}|^2}{\omega_{\boldsymbol{k}\lambda}}\delta(\epsilon_{\boldsymbol{k}}-\omega_{\boldsymbol{k}\lambda})\left[1+f_B\left(\frac{\hbar\epsilon_{\boldsymbol{k}}}{k_BT}\right)\right]f_B\left(\frac{\hbar\epsilon_{\boldsymbol{k}}}{k_BT}\right), \tag{C2h}$$

and

$$\Gamma^{(2)}_{\perp} = \frac{\pi\hbar a^3}{mk_B^2T^2V^2}\sum_{\boldsymbol{k}\boldsymbol{k}'\boldsymbol{q}\lambda}\delta_{\lambda,\perp}\omega_{\boldsymbol{q}\lambda}\left\{\delta_{\boldsymbol{k}-\boldsymbol{k}',\boldsymbol{q}}|\hat{\boldsymbol{e}}_{\boldsymbol{q}\lambda}\cdot\boldsymbol{U}_{\boldsymbol{k},\boldsymbol{k}'}|^2\delta(\epsilon_{\boldsymbol{k}}-\epsilon_{\boldsymbol{k}'}-\omega_{\boldsymbol{q}\lambda})\left[1+f_B\left(\frac{\hbar\epsilon_{\boldsymbol{k}}}{k_BT}\right)\right]f_B\left(\frac{\hbar\epsilon_{\boldsymbol{k}'}}{k_BT}\right)f_B\left(\frac{\hbar\omega_{\boldsymbol{q}\lambda}}{k_BT}\right)\right.$$
$$\left.+\,\delta_{\boldsymbol{k}+\boldsymbol{k}',\boldsymbol{q}}\frac{|\hat{\boldsymbol{e}}^*_{\boldsymbol{q}\lambda}\cdot\boldsymbol{V}_{\boldsymbol{k},\boldsymbol{k}'}|^2}{2}\delta(\epsilon_{\boldsymbol{k}}+\epsilon_{\boldsymbol{k}'}-\omega_{\boldsymbol{q}\lambda})\left[1+f_B\left(\frac{\hbar\epsilon_{\boldsymbol{k}}}{k_BT}\right)\right]\left[1+f_B\left(\frac{\hbar\epsilon_{\boldsymbol{k}'}}{k_BT}\right)\right]f_B\left(\frac{\hbar\omega_{\boldsymbol{q}\lambda}}{k_BT}\right)\right\}, \tag{C3a}$$

$$\Gamma^{(2)}_{\parallel} = \frac{\pi\hbar a^3}{mk_B^2T^2V^2}\sum_{\boldsymbol{k}\boldsymbol{k}'\boldsymbol{q}\lambda}\delta_{\lambda,\parallel}\omega_{\boldsymbol{q}\lambda}\left\{\delta_{\boldsymbol{k}-\boldsymbol{k}',\boldsymbol{q}}|\hat{\boldsymbol{e}}_{\boldsymbol{q}\lambda}\cdot\boldsymbol{U}_{\boldsymbol{k},\boldsymbol{k}'}|^2\delta(\epsilon_{\boldsymbol{k}}-\epsilon_{\boldsymbol{k}'}-\omega_{\boldsymbol{q}\lambda})\left[1+f_B\left(\frac{\hbar\epsilon_{\boldsymbol{k}}}{k_BT}\right)\right]f_B\left(\frac{\hbar\epsilon_{\boldsymbol{k}'}}{k_BT}\right)f_B\left(\frac{\hbar\omega_{\boldsymbol{q}\lambda}}{k_BT}\right)\right.$$
$$\left.+\,\delta_{\boldsymbol{k}+\boldsymbol{k}',\boldsymbol{q}}\frac{|\hat{\boldsymbol{e}}^*_{\boldsymbol{q}\lambda}\cdot\boldsymbol{V}_{\boldsymbol{k},\boldsymbol{k}'}|^2}{2}\delta(\epsilon_{\boldsymbol{k}}+\epsilon_{\boldsymbol{k}'}-\omega_{\boldsymbol{q}\lambda})\left[1+f_B\left(\frac{\hbar\epsilon_{\boldsymbol{k}}}{k_BT}\right)\right]\left[1+f_B\left(\frac{\hbar\epsilon_{\boldsymbol{k}'}}{k_BT}\right)\right]f_B\left(\frac{\hbar\omega_{\boldsymbol{q}\lambda}}{k_BT}\right)\right\}, \tag{C3b}$$

$$\Gamma^{(2)}_{v} = \frac{\pi\hbar a^3c_\perp^2}{mk_B^2T^2V^2}\sum_{\boldsymbol{k}\boldsymbol{k}'\boldsymbol{q}\lambda}\delta_{\lambda,\perp}(q^z)^2\left\{\delta_{\boldsymbol{k}-\boldsymbol{k}',\boldsymbol{q}}\frac{|\hat{\boldsymbol{e}}_{\boldsymbol{q}\lambda}\cdot\boldsymbol{U}_{\boldsymbol{k},\boldsymbol{k}'}|^2}{\omega_{\boldsymbol{q}\lambda}}\delta(\epsilon_{\boldsymbol{k}}-\epsilon_{\boldsymbol{k}'}-\omega_{\boldsymbol{q}\lambda})\left[1+f_B\left(\frac{\hbar\epsilon_{\boldsymbol{k}}}{k_BT}\right)\right]f_B\left(\frac{\hbar\epsilon_{\boldsymbol{k}'}}{k_BT}\right)f_B\left(\frac{\hbar\omega_{\boldsymbol{q}\lambda}}{k_BT}\right)\right.$$
$$\left.+\,\delta_{\boldsymbol{k}+\boldsymbol{k}',\boldsymbol{q}}\frac{|\hat{\boldsymbol{e}}^*_{\boldsymbol{q}\lambda}\cdot\boldsymbol{V}_{\boldsymbol{k},\boldsymbol{k}'}|^2}{2\omega_{\boldsymbol{q}\lambda}}\delta(\epsilon_{\boldsymbol{k}}+\epsilon_{\boldsymbol{k}'}-\omega_{\boldsymbol{q}\lambda})\left[1+f_B\left(\frac{\hbar\epsilon_{\boldsymbol{k}}}{k_BT}\right)\right]\left[1+f_B\left(\frac{\hbar\epsilon_{\boldsymbol{k}'}}{k_BT}\right)\right]f_B\left(\frac{\hbar\omega_{\boldsymbol{q}\lambda}}{k_BT}\right)\right\}, \tag{C3c}$$

$$\Gamma^{(2)}_{\perp v} = \frac{\pi\hbar a^3c_\perp}{mk_B^2T^2V^2}\sum_{\boldsymbol{k}\boldsymbol{k}'\boldsymbol{q}\lambda}\delta_{\lambda,\perp}\lambda q^z\left\{\delta_{\boldsymbol{k}-\boldsymbol{k}',\boldsymbol{q}}|\hat{\boldsymbol{e}}_{\boldsymbol{q}\lambda}\cdot\boldsymbol{U}_{\boldsymbol{k},\boldsymbol{k}'}|^2\delta(\epsilon_{\boldsymbol{k}}-\epsilon_{\boldsymbol{k}'}-\omega_{\boldsymbol{q}\lambda})\left[1+f_B\left(\frac{\hbar\epsilon_{\boldsymbol{k}}}{k_BT}\right)\right]f_B\left(\frac{\hbar\epsilon_{\boldsymbol{k}'}}{k_BT}\right)f_B\left(\frac{\hbar\omega_{\boldsymbol{q}\lambda}}{k_BT}\right)\right.$$
$$\left.+\,\delta_{\boldsymbol{k}+\boldsymbol{k}',\boldsymbol{q}}\frac{|\hat{\boldsymbol{e}}^*_{\boldsymbol{q}\lambda}\cdot\boldsymbol{V}_{\boldsymbol{k},\boldsymbol{k}'}|^2}{2}\delta(\epsilon_{\boldsymbol{k}}+\epsilon_{\boldsymbol{k}'}-\omega_{\boldsymbol{q}\lambda})\left[1+f_B\left(\frac{\hbar\epsilon_{\boldsymbol{k}}}{k_BT}\right)\right]\left[1+f_B\left(\frac{\hbar\epsilon_{\boldsymbol{k}'}}{k_BT}\right)\right]f_B\left(\frac{\hbar\omega_{\boldsymbol{q}\lambda}}{k_BT}\right)\right\}, \tag{C3d}$$

$$\Gamma^{(2)}_{\perp\mu} = -\frac{\pi a^3}{mk_BTV^2}\sum_{\boldsymbol{k}\boldsymbol{k}'\boldsymbol{q}\lambda}\delta_{\lambda,\perp}\delta_{\boldsymbol{k}+\boldsymbol{k}',\boldsymbol{q}}|\hat{\boldsymbol{e}}^*_{\boldsymbol{q}\lambda}\cdot\boldsymbol{V}_{\boldsymbol{k},\boldsymbol{k}'}|^2\delta(\epsilon_{\boldsymbol{k}}+\epsilon_{\boldsymbol{k}'}-\omega_{\boldsymbol{q}\lambda})\left[1+f_B\left(\frac{\hbar\epsilon_{\boldsymbol{k}}}{k_BT}\right)\right]\left[1+f_B\left(\frac{\hbar\epsilon_{\boldsymbol{k}'}}{k_BT}\right)\right]f_B\left(\frac{\hbar\omega_{\boldsymbol{q}\lambda}}{k_BT}\right), \tag{C3e}$$

$$\Gamma^{(2)}_{\parallel\mu} = -\frac{\pi a^3}{mk_BTV^2}\sum_{\boldsymbol{k}\boldsymbol{k}'\boldsymbol{q}\lambda}\delta_{\lambda,\parallel}\delta_{\boldsymbol{k}+\boldsymbol{k}',\boldsymbol{q}}|\hat{\boldsymbol{e}}^*_{\boldsymbol{q}\lambda}\cdot\boldsymbol{V}_{\boldsymbol{k},\boldsymbol{k}'}|^2\delta(\epsilon_{\boldsymbol{k}}+\epsilon_{\boldsymbol{k}'}-\omega_{\boldsymbol{q}\lambda})\left[1+f_B\left(\frac{\hbar\epsilon_{\boldsymbol{k}}}{k_BT}\right)\right]\left[1+f_B\left(\frac{\hbar\epsilon_{\boldsymbol{k}'}}{k_BT}\right)\right]f_B\left(\frac{\hbar\omega_{\boldsymbol{q}\lambda}}{k_BT}\right), \tag{C3f}$$

$$\Gamma^{(2)}_{v\mu} = -\frac{\pi a^3c_\perp}{mk_BTV^2}\sum_{\boldsymbol{k}\boldsymbol{k}'\boldsymbol{q}\lambda}\delta_{\lambda,\perp}\delta_{\boldsymbol{k}+\boldsymbol{k}',\boldsymbol{q}}\lambda q^z\frac{|\hat{\boldsymbol{e}}^*_{\boldsymbol{q}\lambda}\cdot\boldsymbol{V}_{\boldsymbol{k},\boldsymbol{k}'}|^2}{\omega_{\boldsymbol{q}\lambda}}\delta(\epsilon_{\boldsymbol{k}}+\epsilon_{\boldsymbol{k}'}-\omega_{\boldsymbol{q}\lambda})\left[1+f_B\left(\frac{\hbar\epsilon_{\boldsymbol{k}}}{k_BT}\right)\right]\left[1+f_B\left(\frac{\hbar\epsilon_{\boldsymbol{k}'}}{k_BT}\right)\right]f_B\left(\frac{\hbar\omega_{\boldsymbol{q}\lambda}}{k_BT}\right), \tag{C3g}$$

$$\Gamma^{(2)}_{\mu} = \frac{2\pi a^3}{\hbar mV^2}\sum_{\boldsymbol{k}\boldsymbol{k}'\boldsymbol{q}\lambda}\delta_{\boldsymbol{k}+\boldsymbol{k}',\boldsymbol{q}}\frac{|\hat{\boldsymbol{e}}^*_{\boldsymbol{q}\lambda}\cdot\boldsymbol{V}_{\boldsymbol{k},\boldsymbol{k}'}|^2}{\omega_{\boldsymbol{q}\lambda}}\delta(\epsilon_{\boldsymbol{k}}+\epsilon_{\boldsymbol{k}'}-\omega_{\boldsymbol{q}\lambda})\left[1+f_B\left(\frac{\hbar\epsilon_{\boldsymbol{k}}}{k_BT}\right)\right]\left[1+f_B\left(\frac{\hbar\epsilon_{\boldsymbol{k}'}}{k_BT}\right)\right]f_B\left(\frac{\hbar\omega_{\boldsymbol{q}\lambda}}{k_BT}\right), \tag{C3h}$$

where $\delta_{\lambda,\perp} = \delta_{\lambda,+} + \delta_{\lambda,-}$.

[1] K. Uchida, J. Xiao, H. Adachi, J. Ohe, S. Takahashi, J. Ieda, T. Ota, Y. Kajiwara, H. Umezawa, H. Kawai, G. E. W. Bauer, S. Maekawa, and E. Saitoh, Spin Seebeck insulator, Nat. Mater. **9**, 894 (2010).

[2] J. Xiao, G. E. W. Bauer, K. Uchida, E. Saitoh, and S. Maekawa, Theory of magnon-driven spin Seebeck effect, Phys. Rev. B **81**, 214418 (2010).

[3] C. M. Jaworski, J. Yang, S. Mack, D. D. Awschalom, R. C. Myers, and J. P. Heremans, Spin-Seebeck Effect: A Phonon Driven Spin Distribution, Phys. Rev. Lett. **106**, 186601 (2011).

[4] K. Uchida, H. Adachi, T. An, T. Ota, M. Toda, B. Hillebrands, S. Maekawa, and E. Saitoh, Long-range spin Seebeck effect and acoustic spin pumping, Nat. Mater. **10**, 737 (2011).

[5] T. Kikkawa, K. Shen, B. Flebus, R. A. Duine, K. Uchida, Z. Qiu, G. E. W. Bauer, and E. Saitoh, Magnon Polarons in the Spin Seebeck Effect, Phys. Rev. Lett. **117**, 207203 (2016).

[6] R. Schmidt, F. Wilken, T. S. Nunner, and P. W. Brouwer, Boltzmann approach to the longitudinal spin Seebeck effect, Phys. Rev. B **98**, 134421 (2018).

[7] S. Streib, N. Vidal-Silva, K. Shen, and G. E. W. Bauer, Magnon-phonon interactions in magnetic insulators, Phys. Rev. B **99**, 184442 (2019).

[8] A. Einstein and W. J. de Haas, Experimenteller nachweis der ampèreschen molekularströme, Verh. Dtsch. Phys. Ges. **17**, 152 (1915).

[9] S. J. Barnett, Magnetization by rotation, Phys. Rev. **6**, 239 (1915).

[10] R. Jaafar, E. M. Chudnovsky, and D. A. Garanin, Dynamics of the Einstein-de Haas effect: Application to a magnetic cantilever, Phys. Rev. B **79**, 104410 (2009).

[11] D. A. Garanin and E. M. Chudnovsky, Angular momentum in spin-phonon processes, Phys. Rev. B **92**, 024421 (2015).

[12] C. Dornes, Y. Acremann, M. Savoini, M. Kubli, M. J. Neugebauer, E. Abreu, L. Huber, G. Lantz, C. A. F. Vaz, H. Lemke, E. M. Bothschafter, M. Porer, V. Esposito, L. Rettig, M. Buzzi, A. Alberca, Y. W. Windsor, P. Beaud, U. Staub, D. Zhu, S. Song, J. M. Glownia, and S. L. Johnson, The ultrafast Einstein-de Haas effect, Nature (London) **565**, 209 (2019).

[13] J. H. Mentink, M. I. Katsnelson, and M. Lemeshko, Quantum many-body dynamics of the Einstein-de Haas effect, Phys. Rev. B **99**, 064428 (2019).

[14] S. V. Vonsovskii and M. S. Svirskii, Phonon Spin, Sov. Phys. Solid State **3**, 1568 (1962).

[15] A. T. Levine, A note concerning the spin of the phonon, Nuovo Cimento **26**, 190 (1962).

[16] J. Holanda, D. S. Maior, A. Azevodo, and S. M. Rezende, Detecting the phonon spin in magnon-phonon conversion experiments, Nat. Phys. **14**, 500 (2018).

[17] L. Zhang and Q. Niu, Angular Momentum of Phonons and the Einstein-de Haas Effect, Phys. Rev. Lett. **112**, 085503 (2014).

[18] J. J. Nakane and H. Kohno, Angular momentum of phonons and its application to single-spin relaxation, Phys. Rev. B **97**, 174403 (2018).

[19] M. Hamada, E. Minamitani, M. Hirayama, and S. Murakami, Phonon Angular Momentum Induced by the Temperature Gradient, Phys. Rev. Lett. **121**, 175301 (2018).

[20] S. Streib, H. Keshtgar, and G. E. W. Bauer, Damping of Magnetization Dynamics by Phonon Pumping, Phys. Rev. Lett. **121**, 027202 (2018).

[21] D. M. Juraschek and N. A. Spaldin, Orbital magnetic moments of phonons, Phys. Rev. Mater. **3**, 064405 (2019).

[22] C. C. Rusconi and O. Romero-Isart, Magnetic rigid rotor in the quantum regime: Theoretical toolbox, Phys. Rev. B **93**, 054427 (2016).

[23] J. Prat-Camps, C. Teo, C. C. Rusconi, W. Wieczorek, and O. Romero-Isart, Ultrasensitive Inertial and Force Sensors with Diamagnetically Levitated Magnets, Phys. Rev. Appl. **8**, 034002 (2017).

[24] C. C. Rusconi, V. Pöchhacker, K. Kustura, J. I. Cirac, and O. Romero-Isart, Quantum Spin Stabilized Magnetic Levitation, Phys. Rev. Lett. **119**, 167202 (2017).

[25] C. Gonzalez-Ballestero, J. Gieseler, O. Romero-Isart, Quantum acoustomechanics with a micromagnet, arXiv:1907.04039.

[26] K. An, A. N. Litvinenko, R. Kohno, A. A. Fuad, V. V. Naletov, L. Vila, U. Ebels, G. de Loubens, H. Hurdequint, N. Beaulieu, J. B. Youssef, N. Vukadinovic, G. E. W. Bauer, A. N. Slavin, V. S. Tiberkevich, and O. Klein, Coherent long-range transfer of angular momentum between magnon Kittel modes by phonons, Phys. Rev. B **101**, 060407(R) (2020).

[27] D. E. Eastman, Ultrasonic study of first-order and second-order magnetoelastic properties of yttrium iron garnet, Phys. Rev. **148**, 530 (1966).

[28] A. G. Gurevich and G. A. Melkov, *Magnetization Oscillations and Waves* (CRC Press, Boca Raton, 1996).

[29] H. F. Tiersten, Coupled magnetomechanical equations for magnetically saturated insulators, J. Math. Phys. **5**, 1298 (1964).

[30] H. F. Tiersten, Variational principle for saturated magnetoelastic insulators, J. Math. Phys. **6**, 779 (1965).

[31] R. L. Melcher, Rotationally Invariant Theory of Spin-Phonon Interactions in Paramagnets, Phys. Rev. Lett. **28**, 165 (1972); Elastic properties of a paramagnet: Application to $NdVO_4$, Phys. Rev. B **19**, 284 (1979).

[32] L. Bonsall and R. L. Melcher, Rotational invariance, finite strain theory, and spin-lattice interactions in paramagnets; application to the rare-earth vanadates, Phys. Rev. B **14**, 1128 (1976).

[33] E. M. Chudnovsky, D. A. Garanin, and R. Schilling, Universal mechanism of spin relaxation in solids, Phys. Rev. B **72**, 094426 (2005).

[34] A. A. Kovalev, G. E. W. Bauer, and A. Brataas, Nanomechanical Magnetization Reversal, Phys. Rev. Lett. **94**, 167201 (2005).

[35] A. A. Kovalev, G. E. W. Bauer, and A. Brataas, Current-driven ferromagnetic resonance, mechanical torques, and rotary motion in magnetic nanostructures, Phys. Rev. B **75**, 014430 (2007).

[36] S. Bretzel, G. E. W. Bauer, Y. Tserkovnyak, and A. Brataas, Barnett effect in thin magnetic films and nanostructures, Appl. Phys. Lett. **95**, 122504 (2009).

[37] E. M. Chudnovsky and R. Jaafar, Electromechanical magnetization switching, J. Appl. Phys. **117**, 103910 (2015).

[38] M. Aßmann and U. Nowak, Spin-lattice relaxation beyond Gilbert damping, J. Magn. Magn. Mater. **469**, 217 (2019).

[39] C. Eckart, Some studies concerning rotating axes and polyatomic molecules, Phys. Rev. **47**, 552 (1935).

[40] J. D. Louck, Derivation of the molecular vibration-rotation Hamiltonian from the Schrödinger equation for the molecular model, J. Mol. Spec. **61**, 107 (1976).

[41] R. G. Littlejohn and M. Reinsch, Gauge fields in the separation of rotations and internal motions in the *n*-body problem, Rev. Mod. Phys. **69**, 213 (1997).

[42] J. K. G. Watson, Simplification of the molecular vibration-rotation hamiltonian, Mol. Phys. **15**, 479 (1968).

[43] J. H. Van Vleck, The coupling of angular momentum vectors in molecules, Rev. Mod. Phys. **23**, 213 (1951).

[44] T. Holstein and H. Primakoff, Field dependence of the intrinsic domain magnetization of a ferromagnet, Phys. Rev. **58**, 1098 (1940).

[45] A. G. McLellan, Angular momentum states for phonons and a rotationally invariant development of lattice dynamics, J. Phys. C: Solid State Phys. **21**, 1177 (1988).

[46] A. Rückriegel, P. Kopietz, D. A. Bozhko, A. A. Serga, and B. Hillebrands, Magnetoelastic modes and lifetime of magnons in thin yttrium iron garnet films, Phys. Rev. B **89**, 184413 (2014).

[47] B. Flebus, K. Shen, T. Kikkawa, K.-i. Uchida, Z. Qiu, E. Saitoh, R. A. Duine, and G. E. W. Bauer, Magnon-polaron transport in magnetic insulators, Phys. Rev. B **95**, 144420 (2017).

[48] L. J. Cornelissen, K. J. H. Peters, G. E. W. Bauer, R. A. Duine, and B. J. van Wees, Magnon spin transport driven by the magnon chemical potential in a magnetic insulator, Phys. Rev. B **94**, 014412 (2016).

[49] V. Cherepanov, I. Kolokolov, and V. L'vov, The saga of YIG: spectra, thermodynamics, interaction and relaxation of magnons in a complex magnet, Phys. Rep. **229**, 81 (1993).

[50] H. Maier-Flaig, S. Klingler, C. Dubs, O. Surzhenko, R. Gross, M. Weiler, H. Huebl, and S. T. B. Goennenwein, Temperature-dependent magnetic damping of yttrium iron garnet spheres, Phys. Rev. B **95**, 214423 (2017).

[51] T. M. Wallis, J. Moreland, and P. Kabos, Einstein-de Haas effect in a NiFe film deposited on a microcantilever, Appl. Phys. Lett. **89**, 122502 (2006).

[52] G. Zolfagharkhani, A. Gaidarzhy, P. Degiovanni, S. Kettemann, P. Fulde, and P. Mohanty, Nanomechanical detection of itinerant electron spin flip, Nat. Nanotechnol. **3**, 720 (2008).

[53] K. Harii, Y. Seo, Y. Tsutsumi, H. Chudo, K. Oyanagi, M. Matsuo, Y. Shiomi, T. Ono, S. Maekawa, and E. Saitoh, Spin Seebeck mechanical force, Nat. Commun. **10**, 2616 (2019).

[54] J. Tejada, R. D. Zysler, E. Molins, and E. M. Chudnovsky, Evidence for Quantization of Mechanical Rotation of Magnetic Nanoparticles, Phys. Rev. Lett. **104**, 027202 (2010).